Acta Mech
https://doi.org/10.1007/s00707-025-04465-9

ORIGINAL PAPER

Amir Gordouei Milan · Mojtaba Ayatollahi · Reza Teymoori Faal · Magd Abdel-Wahab

Mixed-mode problem of multiple interacting embedded and edge cracks in a piezoelectric strip under in-plane electro-mechanical loadings

Received: 7 May 2025 / Revised: 11 June 2025 / Accepted: 14 July 2025

Abstract In-plane analysis of a piezoelectric layer with several embedded and edge cracks is conducted using the distributed dislocation technique. The modeling of the crack is done by employing the continuous distribution of dislocations along its surface. By applying the integral transform method, we derived the stress and electric displacement fields induced by Volterra climb and glide edge dislocations, as well as electric dislocations, in the piezoelectric strip. These fields are employed to formulate integral equations governing the behavior of a cracked piezoelectric strip under in-plane electro-mechanical loading. The singular integral equations with the well-known Cauchy-type singularity are numerically solved for the dislocation density functions by generalizing a numerical method to obtain field intensity factors at the tips of embedded and edge cracks. Several examples are analyzed to investigate the fracture behavior of a piezoelectric strip weakened by edge and embedded cracks with various orientations. The effects of crack orientation, crack location, and electromechanical loading parameters under various mixed-mode conditions are investigated on Mode I and II stress intensity factors, as well as electric displacement intensity factors, for multiple interacting embedded and edge cracks. This study presents a novel analytical solution for the simultaneous modeling of embedded and edge cracks in a piezoelectric strip under mixed-mode loading conditions, a problem not previously addressed in the literature. Furthermore, the related problem is formulated for an arbitrary straight crack, which can also be used to analyze curved cracks.

1 Introduction

A class of anisotropic dielectrics includes piezoelectric materials, wherein electrical and mechanical fields are intrinsically coupled [1, 2]. Certain materials, such as ceramics, have exhibited ferroelectric properties, which enable them to retain electric polarization after external electric fields are removed [1, 2]. In contrast, others, such as quartz, have not displayed ferroelectric behavior and thus lack those polarization memories, limiting their applications that require non-volatile electric states [1, 2]. Piezoelectric materials have been broadly utilized in engineering structures because of their inherent mechanical-electric coupling effects [1, 2]. They have served as sensors by detecting a structure's response by measuring electric charge [1, 2].

A. G. Milan · M. Ayatollahi (✉) · R. T. Faal
Faculty of Engineering, University of Zanjan, P. O. Box 45195-313, Zanjan, Iran
e-mail: mo_ayatollahi@znu.ac.ir

M. Abdel-Wahab
Soete Laboratory, Department of Electrical Energy, Metals, Mechanical Constructions and Systems, Faculty of Engineering and Architecture, Ghent University, Ghent, Belgium

M. Abdel-Wahab
College of Engineering, Yuan Ze University, Taoyuan City, Taiwan

M. Abdel-Wahab
Parallel and Distributed Systems Laboratory, Jožef Stefan Institute, Jamova Cesta 39, 1000 Ljubljana, Slovenia

Published online: 13 August 2025

Excessive responses have been mitigated by applying some additional electric or thermal actuation forces [1, 2]. Integrating the sensing and actuating capabilities of these materials, which adapt to or correct changing operating conditions, has enabled the development of intelligent structures and systems [1, 2]. Furthermore, piezoelectric materials can be embedded in wind turbine blades or towers to harvest vibrational energy caused by wind-induced motion or mechanical operation [3]. In recent years, a significant interest has appeared in some smart structures utilizing discrete piezoelectric patches for controlling structural responses. [1, 2]. Due to their inherent brittle nature and the presence of micro and macro cracks, fracture analysis has been essential and has received significant attention [1]. Numerous studies have been published in journals focusing on the fracture behavior of cracked piezoelectric materials. While we cannot review all these papers here, readers can find additional research in the references we have cited [4–24]. Permeable and impermeable conditions on crack surfaces are frequently utilized in piezoelectric mediums due to challenges in accurately modeling electric boundary conditions on crack surfaces [15, 18]. Fracture analysis in an infinite piezoelectric plane with a crack has been a popular topic of research [15]. Most studies on mixed-mode fracture have been focused exclusively on infinite planes with a single crack, which limits the applicability of their findings to cases involving multiple cracks with various patterns [4]. In this review, we will discuss some of these studies. Sosa and Pak [4] have investigated the fracture behavior of a piezoelectric medium containing a crack. Their studies have reported singularities at crack tips, with typical square root behavior for the stress and electric displacement components. The issue of several cracks in a piezoelectric medium is discussed by Zhang and Hack [5]. Han and Chen [6] have investigated a piezoelectric medium containing parallel cracks, assuming the surfaces of the cracks are impermeable, using the pseudo-traction-electric displacement method. The study found that electric displacement loading had a more significant effect on the strain energy release rate than on the Mode I stress intensity factor. Han and Wang have considered piezoelectric materials with multiple cracks under mode-I condition by employing the distributed dislocation technique. [7]. Chao and Huang [8] have proposed a failure criterion for a cracked infinite piezoelectric medium under permeable conditions on its surface by utilizing the equivalent inclusion method. Gao [9] has investigated a two-dimensional piezoelectric medium weakened by defects using precise boundary conditions. Hao [10] has analyzed the problem of multiple collinear cracks in a piezoelectric medium, assuming the permittivity of air within the cracks. Yang [11] has derived a closed-form solution for a crack in an infinite piezoelectric material under Mode I conditions. Han and Wang [12], have addressed the mode-I problem in a piezoelectric medium that was weakened by a periodic array of cracks under electromechanical loads. Zhou et al. [13] have investigated the Mode-I behavior of multiple parallel cracks in an infinite piezoelectric plane. They have calculated the field intensity factors using the dislocation method at the tips of four interacting parallel cracks. Li and Lee [14] have investigated a piezoelectric plane containing two interacting, unequal, collinear cracks subjected to Mode I electromechanical loading. Research has started employing the well-established distributed dislocation method to evaluate the fracture behavior of infinite piezoelectric planes weakened by multiple cracks. Mahmoudi and Ayatollahi have examined the in-plane problem of multiple interacting cracks in a piezoelectric infinite plane under mixed-mode conditions [15]. Bagheri [16] has analyzed the mixed-mode steady-state problem involving multiple cracks in an infinite functionally graded piezoelectric plane that was subjected to harmonic loading. He has analyzed the effect of material properties, the loading factor, and the interaction of the cracks on the stress and electric displacement intensity factors. The cracked piezoelectric plane under a general in-plane thermal load was the subject of study by Nourazar et al. [17]. Bagheri et al. [18] have determined the stress intensity factors for modes I and II for various crack patterns in a piezoelectric half-plane and studied the interaction between the cracks. They have used the dislocation method to obtain a solution to the mixed-mode crack problem.

Cracked piezoelectric strips have received limited attention due to mathematical challenges associated with them. As a result, the number of publications on this topic is limited in the literature. The problem of an embedded crack in a piezoelectric strip of finite thickness has been examined by Wang and Noda [19]. They applied the strain energy density (SED) criterion. This approach predicts that a crack will initiate and propagate in the direction where the strain energy density factor reaches a critical value, indicating the path of least resistance for crack growth. Wang and Mai [20] have addressed the problem of a cracked piezoelectric strip under in-plane electromechanical loading. Their study examines the effects of crack length and position on stress and electric displacement intensity factors, considering various electric conditions applied to the crack surface. The thermo-electro-elastic behavior of a cracked non-homogeneous piezoelectric layer under mixed-mode conditions has been studied by Ueda [21]. He has determined the stress and electric displacement intensity factors for various values of non-dimensional parameters, which correspond to crack length, crack position, and material non-homogeneity [21]. All the investigations mentioned above have been concentrated on a piezoelectric strip with a single crack [19–21]. The closed-form solution of mode-III deformation for a piezoelectric strip containing two coaxial cracks has been presented by Li [22]. Yang et al. [23] investigated the dynamic response of a piezoelectric strip containing a crack parallel to its boundaries under thermoelectric impact. Li et al. [24] have conducted a fracture analysis of a centrally located crack in a piezoelectric strip subjected to Mode I loading conditions. Boroujerdi and Monfared [25] have conducted a study on the problem of a non-homogeneous piezoelectric strip bonded to a piezoelectric half-plane that contained multiple interfacial cracks with unequal length. They have investigated how the non-homogeneity parameter, material properties, and loading conditions affected the intensity factors at the tips of the cracks. There is limited research available on mixed-mode crack problems in the piezoelectric strips. Specifically, the interactions between multiple embedded and edge cracks occurring simultaneously under these conditions have not been studied. This work develops a novel analytical framework for the simultaneous analysis of interacting embedded and edge cracks of arbitrary number and configuration in a piezoelectric strip subjected to mixed-mode electromechanical loading—an issue that, to the best of the authors' knowledge, has not been previously addressed in the literature. To address this research gap, the present study investigates the mixed-mode electromechanical response of a piezoelectric strip containing multiple interacting embedded and edge cracks. The primary limitation of the proposed methodology is the assumption that crack closure does not occur; therefore, the applied tractions on the crack surfaces must be such that they preclude any partial or full crack face contact.

We use the integral transform technique to find solutions for electric dislocation, as well as for climbing and gliding edge dislocations in the piezoelectric strip. The solutions for dislocations display the familiar Cauchy-type singularity and can be used to analyze multiple cracks in different configurations and arrangements. These solutions are utilized to derive singular integral equations that govern the behavior of electric displacement and traction vectors along crack surfaces in piezoelectric materials. The formulation allows mixed-mode analysis of a piezoelectric layer with several arbitrarily oriented embedded and edge cracks with any smooth geometry.

2 Dislocation solution

In this section, we consider the piezoelectric strip with a given finite thickness h such that, $|x| < \infty$,$0 < y < h$. The constitutive equation for piezoelectric materials regarding mechanical in-plane displacement and electric fields is expressed as [19]:

$$\sigma_{ij} = c_{ijkl}u_{k,l} + e_{lij}\varphi_{,l}$$

$$D_i = e_{ikl}u_{k,l} - \varepsilon_{il}\varphi_{,l} \tag{1}$$

where σ_{ij}, u_i, $D_i(i,\ j = x,\ y)$ and φ are stresses, displacements, electric displacements, and electric potential, respectively. Furthermore, c_{ijkl}, e_{ijk} and ε_{il} are elastic constants, piezoelectric constants, and dielectric constants, respectively. Partial derivatives are indicated using a comma. This study involves polarization of the piezoelectric material in the y-direction. Thus, by neglecting body forces and free electric charges, we derive the governing equations from the equilibrium equation as follows: [15]

$$c_{11}u_{,xx} + c_{44}u_{,yy} + (c_{13} + c_{44})v_{,xy} + (e_{31} + e_{15})\varphi_{,xy} = 0,$$

$$c_{44}v_{,xx} + c_{33}v_{,yy} + (c_{13} + c_{44})u_{,xy} + e_{15}\varphi_{,xx} + e_{33}\varphi_{,yy} = 0,$$

$$e_{15}v_{,xx} + e_{33}v_{,yy} + (e_{31} + e_{15})u_{,xy} - \varepsilon_{11}\varphi_{,xx} - \varepsilon_{33}\varphi_{,yy} = 0. \tag{2}$$

The initial step in solving the crack problem is to find a solution for dislocations. To achieve this, we consider a piezoelectric strip with a given thickness h weakened by an electro-elastic dislocation located at arbitrary coordinates $(\xi,\ \eta)$. The boundaries of the piezoelectric strip are traction and charge-free, i.e.:

$$\sigma_{yy}(x,\ 0) = 0, \quad \sigma_{xy}(x,\ 0) = 0, \quad D_y(x,\ 0) = 0$$

$$\sigma_{yy}(x, h) = 0, \quad \sigma_{xy}(x, h) = 0, \quad D_y(x, h) = 0, \tag{3}$$

The dislocation problem must be solved subject to the following multi-valued conditions for climb and glide edge dislocation with constants Burgers vectors b_y and b_x, respectively,:

$$u(x,\ \eta^+) - u(x,\ \eta^-) = b_x H(x - \xi)$$

$$v(x,\eta^{+})-v(x,\eta^{-})=b_{y}H(x-\zeta) \tag{4}$$

where $H(.)$ is the Heaviside step function in Eq. (4). Additionally, the electrical potential discontinuity which introduces the electroelastic dislocation, is as follows [2]:

$$\varphi(x,\eta^{+})-\varphi(x,\eta^{-})=b_{\varphi}H(x-\zeta) \tag{5}$$

While the multi-valued electric potential is not categorized as a dislocation, it is frequently referred to as an electric dislocation with a Burgers vector b_{φ}. In the context of permeability, the changes in electric potential are assumed to be zero. Along the dislocation line, the continuity of stress components and electric displacement is represented by:

$$\begin{aligned}
&\sigma_{xy}(x,\ \eta^{+})=\sigma_{xy}(x,\ \eta^{-})\\
&\sigma_{yy}(x,\ \eta^{+})=\sigma_{yy}(x,\ \eta^{-})\\
&D_{y}(x,\eta^{+})=D_{y}(x,\eta^{-})
\end{aligned} \tag{6}$$

In this analysis, we will utilize the Fourier transform. Application of the complex Fourier transforms to Eq. (2), leads to:

$$\begin{aligned}
&c_{44}\frac{d^{2}U}{dy^{2}}-c_{11}s^{2}U-is(c_{13}+c_{44})\frac{dV}{dy}-is(e_{31}+e_{15})\frac{d\Phi}{dy}=0,\\
&c_{33}\frac{d^{2}V}{dy^{2}}-c_{44}s^{2}V-is(c_{13}+c_{44})\frac{dU}{dy}-e_{15}s^{2}\Phi+e_{33}\frac{d^{2}\Phi}{dy^{2}}=0,\\
&e_{33}\frac{d^{2}V}{dy^{2}}-s^{2}e_{15}V-is(e_{31}+e_{15})\frac{dU}{dy}+\varepsilon_{11}s^{2}\Phi-\varepsilon_{33}\frac{d^{2}\Phi}{dy^{2}}=0.
\end{aligned} \tag{7}$$

In Eqs. (7), the functions $U(s,\ y)$,$V(s,\ y)$ and $\Phi(s,\ y)$ represent the Fourier transform of $u(x,\ y)$, $v(x,\ y)$ and $\varphi(x,\ y)$, respectively. Equation (7) admits a straightforward solution.

$$\begin{aligned}
&U_{k}(s,\ y)=\sum_{j=1}^{3}(A_{kj}e^{-|s|\lambda_{j}y}+B_{kj}e^{|s|\lambda_{j}y})\\
&V_{k}(s,\ y)=i\,\mathrm{sgn}(s)\sum_{j=1}^{3}m_{j1}(A_{kj}e^{-|s|\lambda_{j}y}-B_{kj}e^{|s|\lambda_{j}y})\\
&\Phi_{k}(s,y)=i\,\mathrm{sgn}(s)\sum_{j=1}^{3}m_{j2}(A_{kj}e^{-|s|\lambda_{j}y}-B_{kj}e^{|s|\lambda_{j}y}),\qquad k=1,2
\end{aligned} \tag{8}$$

where λ_{j} represent the roots of the characteristic equation resulting from Eq. (7) and $m_{jl},\quad l\in\{1,2\}$ is defined as follows:

$$m_{j1}=\frac{c_{44}\varepsilon_{33}\lambda_{j}^{4}+\mu_{1}\lambda_{j}^{2}+c_{11}\varepsilon_{11}}{\mu_{2}\lambda_{j}^{3}+\mu_{3}\lambda_{j}},\quad m_{j2}=\frac{c_{44}\lambda_{j}^{2}-(c_{13}+c_{44})\lambda_{j}m_{j1}-c_{11}}{(e_{31}+e_{15})\lambda_{j}},\quad j\in\{1,2,3\} \tag{9}$$

in which

$$\begin{aligned}
&\mu_{1}=-c_{11}\varepsilon_{33}-(e_{31}+e_{15})^{2}-c_{44}\varepsilon_{11},\\
&\mu_{2}=e_{33}(e_{31}+e_{15})+(c_{13}+c_{44})\varepsilon_{33},\\
&\mu_{3}=-e_{15}(e_{31}+e_{15})-(c_{13}+c_{44})\varepsilon_{11}.
\end{aligned} \tag{10}$$

In Eq. (8), subscripts $k=1$ and $k=2$ indicate regions $0<y<\eta$ and $\eta<y<h$, respectively. Utilizing Eqs. (1) and (8), the Fourier transform of stress components and electric displacements could be derived as:

$$\sigma_{xxk}(s,\ y) = -is\sum_{j=1}^{3} m_{j3}(A_{kj}e^{-|s|\lambda_j y} + B_{kj}e^{|s|\lambda_j y})$$
$$\sigma_{yyk}(s,\ y) = -is\sum_{j=1}^{3} m_{j4}(A_{kj}e^{-|s|\lambda_j y} + B_{kj}e^{|s|\lambda_j y})$$
$$\sigma_{xyk}(s,\ y) = |s|\sum_{j=1}^{3} m_{j5}(A_{kj}e^{-|s|\lambda_j y} - B_{kj}e^{|s|\lambda_j y})$$
$$D_{xk}(s,\ y) = |s|\sum_{j=1}^{3} m_{j6}(A_{kj}e^{-|s|\lambda_j y} - B_{kj}e^{|s|\lambda_j y})$$
$$D_{yk}(s, y) = -is\sum_{j=1}^{3} m_{j7}(A_{kj}e^{-|s|\lambda_j y} + B_{kj}e^{|s|\lambda_j y}) \tag{11}$$

The unknown functions A_{kj}, B_{kj}, $(k = 1, 2\ ,\ j = 1, 2, 3)$ may be determined by performing the exponential Fourier transform to conditions (3–6). Moreover, the expressions for m_{j3},m_{j4},m_{j5}, m_{j6} and m_{j7} which appear in (11) are defined in the Appendix. After some lengthy manipulations, we obtain the following expressions:

$$A_{kj}(s) = (E_{kjx}b_x + i\,\mathrm{sgn}(s)E_{kjy}b_y + i\,\mathrm{sgn}(s)E_{kj\varphi}b_\varphi)e^{is\xi}(\pi\delta(s) + i\big/ s)$$
$$B_{kj}(s) = (F_{kjx}b_x + i\,\mathrm{sgn}(s)F_{kjy}b_y + i\,\mathrm{sgn}(s)F_{kj\varphi}b_\varphi)e^{is\xi}(\pi\delta(s) + i\big/ s), \tag{12}$$

where the functions E_{kjl}, and F_{kjl}, $\ (l \in \{x,\ y,\ \varphi\})$; are given in Appendix. The inverse exponential Fourier transform of Eq. (11), combined with Eq. (12), provides the field components as follows:

$$\sigma_{xxk}(x,\ y) = \frac{1}{2\pi}\int_{-\infty}^{+\infty} e^{-is(x-\xi)}\sum_{j=1}^{3} m_{j3}(E_{kjx}b_x + i\,\mathrm{sgn}(s)E_{kjy}b_y + i\,\mathrm{sgn}(s)E_{kj\varphi}b_\varphi)e^{-|s|\lambda_j y}ds$$
$$+\frac{1}{2\pi}\int_{-\infty}^{+\infty} e^{-is(x-\xi)}\sum_{j=1}^{3} m_{j3}(F_{kjx}b_x + i\,\mathrm{sgn}(s)F_{kjy}b_y + i\,\mathrm{sgn}(s)F_{kj\varphi}b_\varphi)e^{-|s|\lambda_j y}ds$$
$$\sigma_{yyk}(x,\ y) = \frac{1}{2\pi}\int_{-\infty}^{+\infty} e^{-is(x-\xi)}\sum_{j=1}^{3} m_{j4}(E_{kjx}b_x + i\,\mathrm{sgn}(s)E_{kjy}b_y + i\,\mathrm{sgn}(s)E_{kj\varphi}b_\varphi)e^{-|s|\lambda_j y}ds$$
$$+\frac{1}{2\pi}\int_{-\infty}^{+\infty} e^{-is(x-\xi)}\sum_{j=1}^{3} m_{j4}(F_{kjx}b_x + i\,\mathrm{sgn}(s)F_{kjy}b_y + i\,\mathrm{sgn}(s)F_{kj\varphi}b_\varphi)e^{-|s|\lambda_j y}ds$$
$$\sigma_{xyk}(x,\ y) = \frac{1}{2\pi}\int_{-\infty}^{+\infty} e^{-is(x-\xi)}\sum_{j=1}^{3} m_{j5}(i\,\mathrm{sgn}(s)E_{kjx}b_x - E_{kjy}b_y - E_{kj\varphi}b_\varphi)e^{-|s|\lambda_j y}ds$$
$$-\frac{1}{2\pi}\int_{-\infty}^{+\infty} e^{-is(x-\xi)}\sum_{j=1}^{3} m_{j5}(i\,\mathrm{sgn}(s)F_{kjx}b_x - F_{kjy}b_y - F_{kj\varphi}b_\varphi)e^{|s|\lambda_j y}ds$$
$$D_{xk}(x,\ y) = \frac{1}{2\pi}\int_{-\infty}^{+\infty} e^{-is(x-\xi)}\sum_{j=1}^{3} m_{j6}(i\,\mathrm{sgn}(s)E_{kjx}b_x - E_{kjy}b_y - E_{kj\varphi}b_\varphi)e^{-|s|\lambda_j y}ds$$
$$-\frac{1}{2\pi}\int_{-\infty}^{+\infty} e^{-is(x-\xi)}\sum_{j=1}^{3} m_{j6}(i\,\mathrm{sgn}(s)F_{kjx}b_x - F_{kjy}b_y - F_{kj\varphi}b_\varphi)e^{|s|\lambda_j y}ds$$

$$D_{yk}(x,y)=\frac{1}{2\pi}\int_{-\infty}^{+\infty}e^{-is(x-\xi)}\sum_{j=1}^{3}m_{j7}(E_{kjx}b_x+i\,\mathrm{sgn}(s)E_{kjy}b_y+i\,\mathrm{sgn}(s)E_{kj\varphi}b_\varphi)e^{-|s|\lambda_j y}ds$$
$$+\frac{1}{2\pi}\int_{-\infty}^{+\infty}e^{-is(x-\xi)}\sum_{j=1}^{3}m_{j7}(F_{kjx}b_x+i\,\mathrm{sgn}(s)F_{kjy}b_y+i\,\mathrm{sgn}(s)F_{kj\varphi}b_\varphi)e^{-|s|\lambda_j y}ds \tag{13}$$

To simplify the integrals in Eq. (13), we divide the integrals into odd and even expressions based on the parameter,s, i.e.:

$$\sigma_{xxk}(x,\ y)=\frac{b_x}{\pi}\int_0^{+\infty}\sum_{j=1}^{3}m_{j3}E_{kjx}\cos[s(x-\xi)]e^{-s\lambda_j y}ds+\frac{b_x}{\pi}\int_0^{+\infty}\sum_{j=1}^{3}m_{j3}F_{kjx}\cos[s(x-\xi)]e^{-s\lambda_j y}ds$$
$$+\frac{b_y}{\pi}\int_0^{+\infty}\sum_{j=1}^{3}m_{j3}E_{kjy}\sin[s(x-\xi)]e^{-s\lambda_j y}ds+\frac{b_y}{\pi}\int_0^{+\infty}\sum_{j=1}^{3}m_{j3}F_{kjy}\sin[s(x-\xi)]e^{-s\lambda_j y}ds$$
$$+\frac{b_\varphi}{\pi}\int_0^{+\infty}\sum_{j=1}^{3}m_{j3}E_{kj\varphi}\sin[s(x-\xi)]e^{-s\lambda_j y}ds+\frac{b_\varphi}{\pi}\int_0^{+\infty}\sum_{j=1}^{3}m_{j3}F_{kj\varphi}\sin[s(x-\xi)]e^{-s\lambda_j y}ds$$

$$\sigma_{yyk}(x,\ y)=\frac{b_x}{\pi}\int_0^{+\infty}\sum_{j=1}^{3}m_{j4}E_{kjx}\cos[s(x-\xi)]e^{-s\lambda_j y}ds+\frac{b_x}{\pi}\int_0^{+\infty}\sum_{j=1}^{3}m_{j4}F_{kjx}\cos[s(x-\xi)]e^{-s\lambda_j y}ds$$
$$+\frac{b_y}{\pi}\int_0^{+\infty}\sum_{j=1}^{3}m_{j4}E_{kjy}\sin[s(x-\xi)]e^{-s\lambda_j y}ds+\frac{b_y}{\pi}\int_0^{+\infty}\sum_{j=1}^{3}m_{j4}F_{kjy}\sin[s(x-\xi)]e^{-s\lambda_j y}ds$$
$$+\frac{b_\varphi}{\pi}\int_0^{+\infty}\sum_{j=1}^{3}m_{j4}E_{kj\varphi}\sin[s(x-\xi)]e^{-s\lambda_j y}ds+\frac{b_\varphi}{\pi}\int_0^{+\infty}\sum_{j=1}^{3}m_{j4}F_{kj\varphi}\sin[s(x-\xi)]e^{-s\lambda_j y}ds$$

$$\sigma_{xyk}(x,\ y)=\frac{b_x}{\pi}\int_0^{+\infty}\sum_{j=1}^{3}m_{j5}E_{kjx}\sin[s(x-\xi)]e^{-s\lambda_j y}ds-\frac{b_x}{\pi}\int_0^{+\infty}\sum_{j=1}^{3}m_{j5}F_{kjx}\sin[s(x-\xi)]e^{s\lambda_j y}ds$$
$$-\frac{b_y}{\pi}\int_0^{+\infty}\sum_{j=1}^{3}m_{j5}E_{kjy}\cos[s(x-\xi)]e^{-s\lambda_j y}ds+\frac{b_y}{\pi}\int_0^{+\infty}\sum_{j=1}^{3}m_{j5}F_{kjy}\cos[s(x-\xi)]e^{s\lambda_j y}ds$$
$$-\frac{b_\varphi}{\pi}\int_0^{+\infty}\sum_{j=1}^{3}m_{j5}E_{kj\varphi}\cos[s(x-\xi)]e^{-s\lambda_j y}ds+\frac{b_\varphi}{\pi}\int_0^{+\infty}\sum_{j=1}^{3}m_{j5}F_{kj\varphi}\cos[s(x-\xi)]e^{s\lambda_j y}ds$$

$$D_{xk}(x,\ y)=\frac{b_x}{\pi}\int_0^{+\infty}\sum_{j=1}^{3}m_{j6}E_{kjx}\sin[s(x-\xi)]e^{-s\lambda_j y}ds-\frac{b_x}{\pi}\int_0^{+\infty}\sum_{j=1}^{3}m_{j6}F_{kjx}\sin[s(x-\xi)]e^{s\lambda_j y}ds$$
$$-\frac{b_y}{\pi}\int_0^{+\infty}\sum_{j=1}^{3}m_{j6}E_{kjy}\cos[s(x-\xi)]e^{-s\lambda_j y}ds+\frac{b_y}{\pi}\int_0^{+\infty}\sum_{j=1}^{3}m_{j6}F_{kjy}\cos[s(x-\xi)]e^{s\lambda_j y}ds$$
$$-\frac{b_\varphi}{\pi}\int_0^{+\infty}\sum_{j=1}^{3}m_{j6}E_{kj\varphi}\cos[s(x-\xi)]e^{-s\lambda_j y}ds+\frac{b_\varphi}{\pi}\int_0^{+\infty}\sum_{j=1}^{3}m_{j6}F_{kj\varphi}\cos[s(x-\xi)]e^{s\lambda_j y}ds$$

$$\begin{aligned}
D_{yk}(x,y) = {} & \frac{b_x}{\pi}\int_0^{+\infty}\sum_{j=1}^{3} m_{j7}E_{kjx}\cos[s(x-\xi)]e^{-s\lambda_j y}ds + \frac{b_x}{\pi}\int_0^{+\infty}\sum_{j=1}^{3} m_{j7}F_{kjx}\cos[s(x-\xi)]e^{-s\lambda_j y}ds \\
& + \frac{b_y}{\pi}\int_0^{+\infty}\sum_{j=1}^{3} m_{j7}E_{kjy}\sin[s(x-\xi)]e^{-s\lambda_j y}ds + \frac{b_y}{\pi}\int_0^{+\infty}\sum_{j=1}^{3} m_{j7}F_{kjy}\sin[s(x-\xi)]e^{-s\lambda_j y}ds \\
& + \frac{b_\varphi}{\pi}\int_0^{+\infty}\sum_{j=1}^{3} m_{j7}E_{kj\varphi}\sin[s(x-\xi)]e^{-s\lambda_j y}ds + \frac{b_\varphi}{\pi}\int_0^{+\infty}\sum_{j=1}^{3} m_{j7}F_{kj\varphi}\sin[s(x-\xi)]e^{-s\lambda_j y}ds
\end{aligned} \tag{14}$$

It can be observed that the integrands in Eq. (14) are continuous functions of s. By applying the asymptotic process to the integrands of the integrals in Eq. (14), we obtain the singular components of the kernels. After some lengthy manipulation, we derive the following asymptotic expressions for large values $s \to \infty$:

$$\begin{aligned}
E_{21x\infty} &= \frac{q_1'}{2Q'}e^{s\lambda_1\eta},\ E_{21y\infty} = -\frac{p_1}{2Q}e^{s\lambda_1\eta},\ E_{21\varphi\infty} = -\frac{p_2}{2Q}e^{s\lambda_1\eta}, \\
E_{22x\infty} &= \frac{q_2'}{2Q'}e^{s\lambda_2\eta},\ E_{22y\infty} = -\frac{p_4}{2Q}e^{s\lambda_2\eta},\ E_{22\varphi\infty} = -\frac{p_5}{2Q}e^{s\lambda_2\eta} \\
E_{23x\infty} &= \frac{q_3'}{2Q'}e^{s\lambda_3\eta},\ E_{23y\infty} = -\frac{p_6}{2Q}e^{s\lambda_3\eta},\ E_{23\varphi\infty} = -\frac{p_7}{2Q}e^{s\lambda_3\eta} \\
F_{11x\infty} &= -\frac{q_1'}{2Q'}e^{-s\lambda_1\eta},\ F_{11y\infty} = -\frac{p_1}{2Q}e^{-s\lambda_1\eta},\ F_{11\varphi\infty} = -\frac{p_2}{2Q}e^{-s\lambda_1\eta} \\
F_{12x\infty} &= -\frac{q_2'}{2Q'}e^{-s\lambda_2\eta},\ F_{12y\infty} = -\frac{p_4}{2Q}e^{-s\lambda_2\eta},\ F_{12\varphi\infty} = -\frac{p_5}{2Q}e^{-s\lambda_2\eta} \\
F_{13x\infty} &= -\frac{q_3'}{2Q'}e^{-s\lambda_3\eta}, F_{13y\infty} = -\frac{p_6}{2Q}e^{-s\lambda_3\eta}, F_{13\varphi\infty} = -\frac{p_7}{2Q}e^{-s\lambda_3\eta},
\end{aligned} \tag{15}$$

The expressions for q_k', $k = 1, 2, 3.$, p_l, $l = 1, 2, ..., 7$, Q; and Q' are given in the Appendix. We employ the following identities

$$\begin{aligned}
\int_0^{+\infty} e^{-s\lambda_i Y}\sin(sX)ds &= \frac{X}{X^2+(\lambda_i Y)^2}, \\
\int_0^{+\infty} e^{-s\lambda_i Y}\cos(sX)ds &= \frac{\lambda_i Y}{X^2+(\lambda_i Y)^2}.
\end{aligned} \tag{16}$$

Then, we first subtract the integrand asymptotic forms Eq. (15) from the integrands Eq. (14) and add these forms again to divide the integrals of the stress and electric fields into two parts. The first part is numerically integrable, and the second part is analytically integrable using Eq. (16).

$$\begin{aligned}
\sigma_{ij}(x,\ y) &= k_{ij}^x b_x + k_{ij}^y b_y + k_{ij}^\varphi b_\varphi \\
D_i(x,y) &= d_i^x b_x + d_i^y b_y + d_i^\varphi b_\varphi, \quad i, j \in \{x, y\}
\end{aligned} \tag{17}$$

The coefficients of b_x, b_y and b_φ are as follows:

$$\begin{aligned}
k_{ll}^x(x,\ y) = {} & \frac{1}{\pi}\int_0^{+\infty}\sum_{i=1}^{3} m_{ir}E_{1ix}e^{-s\lambda_i y}\cos[s(x-\xi)]ds + \frac{1}{\pi}\int_0^{+\infty}\sum_{i=1}^{3} m_{ir}(F_{1ix}-F_{1ix\infty})e^{s\lambda_i y}\cos[s(x-\xi)]ds \\
& + \frac{(y-\eta)}{2\pi Q'}\sum_{i=1}^{3}\frac{m_{ir}q_i'\lambda_i}{(x-\xi)^2+\lambda_i^2(\eta-y)^2}
\end{aligned}$$

$$
\begin{aligned}
k_{ll}^{y}(x,\ y) &= \frac{1}{\pi}\int_0^{+\infty}\sum_{i=1}^{3} m_{ir}E_{1iy}e^{-s\lambda_i y}\sin[s(x-\xi)]ds + \frac{1}{\pi}\int_0^{+\infty}\sum_{i=1}^{3} m_{ir}(F_{1iy}-F_{1iy\infty})e^{s\lambda_i y}\sin[s(x-\xi)]ds \\
&\quad -\frac{1}{2\pi Q}\left[\frac{m_{1r}p_1(x-\xi)}{(x-\xi)^2+\lambda_1^2(\eta-y)^2} + \frac{m_{2r}p_4(x-\xi)}{(x-\xi)^2+\lambda_2^2(\eta-y)^2} + \frac{m_{3r}p_6(x-\xi)}{(x-\xi)^2+\lambda_3^2(\eta-y)^2}\right] \\
k_{ll}^{\varphi}(x,y) &= \frac{1}{\pi}\int_0^{+\infty}\sum_{i=1}^{3} m_{ir}E_{1i\varphi}e^{-s\lambda_i y}\sin[s(x-\xi)]ds + \frac{1}{\pi}\int_0^{+\infty}\sum_{i=1}^{3} m_{ir}(F_{1i\varphi}-F_{1i\varphi\infty})e^{s\lambda_i y}\sin[s(x-\xi)]ds \\
&\quad -\frac{1}{2\pi Q}\left[\frac{m_{1r}p_2(x-\xi)}{(x-\xi)^2+\lambda_1^2(\eta-y)^2} + \frac{m_{2r}p_5(x-\xi)}{(x-\xi)^2+\lambda_2^2(\eta-y)^2} + \frac{m_{3r}p_7(x-\xi)}{(x-\xi)^2+\lambda_3^2(\eta-y)^2}\right]
\end{aligned}
\tag{17}
$$

For $l = x$, $r = 3$ and $l = y$, $r = 4$. Similar relations can be obtained for d_y^x, d_y^y and d_y^{φ} by changing m_{ir} into m_{i7}. Furthermore, we have

$$
\begin{aligned}
k_{xy}^{x}(x,\ y) &= \frac{1}{\pi}\int_0^{+\infty}\sum_{i=1}^{3} m_{i5}E_{1ix}e^{-s\lambda_i y}\sin[(x-\xi)]ds + \frac{1}{\pi}\int_0^{+\infty}\sum_{i=1}^{3} m_{i5}(F_{1ix}-F_{1ix\infty})e^{s\lambda_i y}\sin[(x-\xi)]ds \\
&\quad +\frac{(x-\xi)}{2Q'\pi}\sum_{i=1}^{3}\frac{m_{i5}q_i'}{(x-\xi)^2+[\lambda_i(y-\eta)]^2} \\
k_{xy}^{y}(x,\ y) &= -\frac{1}{\pi}\int_0^{+\infty}\sum_{i=1}^{3} m_{i5}E_{1iy}e^{-s\lambda_i y}\cos[(x-\xi)]ds - \frac{1}{\pi}\int_0^{+\infty}\sum_{i=1}^{3} m_{i5}(F_{1iy}-F_{1iy\infty})e^{s\lambda_i y}\cos[(x-\xi)]ds \\
&\quad +\frac{1}{2Q\pi}\left[\frac{m_{15}p_1\lambda_1(y-\eta)}{(x-\xi)^2+[\lambda_1(y-\eta)]^2} + \frac{m_{25}p_4\lambda_2(y-\eta)}{(x-\xi)^2+[\lambda_2(y-\eta)]^2} + \frac{m_{35}p_6\lambda_3(y-\eta)}{(x-\xi)^2+[\lambda_3(y-\eta)]^2}\right] \\
k_{xy}^{\varphi}(x,y) &= -\frac{1}{\pi}\int_0^{+\infty}\sum_{i=1}^{3} m_{i5}E_{1i\varphi}e^{-s\lambda_i y}\cos[(x-\xi)]ds - \frac{1}{\pi}\int_0^{+\infty}\sum_{i=1}^{3} m_{i5}(F_{1i\varphi}-F_{1i\varphi\infty})e^{s\lambda_i y}\cos[(x-\xi)]ds \\
&\quad +\frac{1}{2Q\pi}\left[\frac{m_{15}p_2\lambda_1(y-\eta)}{(x-\xi)^2+[\lambda_1(y-\eta)]^2} + \frac{m_{25}p_5\lambda_2(y-\eta)}{(x-\xi)^2+[\lambda_2(y-\eta)]^2} - \frac{m_{35}p_7\lambda_3(y-\eta)}{(x-\xi)^2+[\lambda_3(y-\eta)]^2}\right]
\end{aligned}
\tag{18}
$$

By substituting m_{i5} with m_{i6} in Eq. (18), we could derive the expressions for d_y^x, d_y^y and d_y^{φ}. We note that the stress components described in Eqs. (17) and (18) have the Cauchy singularity at the location of the dislocation. In a specific case, by letting $h \to \infty$ in Eqs. (17), the in-plane stress components and electric displacement fields for the infinite piezoelectric plane weakened by an electro-elastic dislocation are obtained as:

$$
\begin{aligned}
\sigma_{xx}(x,\ y) &= \frac{b_x}{2\pi Q'}\left[\frac{m_{13}q_1'\lambda_1(y-\eta)}{(x-\xi)^2+\lambda_1^2(\eta-y)^2} + \frac{m_{23}q_2'\lambda_2(y-\eta)}{(x-\xi)^2+\lambda_2^2(\eta-y)^2} + \frac{m_{33}q_3'\lambda_3(y-\eta)}{(x-\xi)^2+\lambda_3^2(\eta-y)^2}\right] \\
&\quad -\frac{b_y}{2\pi Q}\left[\frac{m_{13}p_1(x-\xi)}{(x-\xi)^2+\lambda_1^2(\eta-y)^2} + \frac{m_{23}p_4(x-\xi)}{(x-\xi)^2+\lambda_2^2(\eta-y)^2} + \frac{m_{33}p_6(x-\xi)}{(x-\xi)^2+\lambda_3^2(\eta-y)^2}\right] \\
&\quad -\frac{b_{\varphi}}{2\pi Q}\left[\frac{m_{13}p_2(x-\xi)}{(x-\xi)^2+\lambda_1^2(\eta-y)^2} + \frac{m_{23}p_5(x-\xi)}{(x-\xi)^2+\lambda_2^2(\eta-y)^2} + \frac{m_{33}p_7(x-\xi)}{(x-\xi)^2+\lambda_3^2(\eta-y)^2}\right] \\
\sigma_{yy}(x,\ y) &= \frac{b_x}{2\pi Q'}\left[\frac{m_{14}q_1'\lambda_1(y-\eta)}{(x-\xi)^2+\lambda_1^2(\eta-y)^2} + \frac{m_{24}q_2'\lambda_2(y-\eta)}{(x-\xi)^2+\lambda_2^2(\eta-y)^2} + \frac{m_{34}q_3'\lambda_3(y-\eta)}{(x-\xi)^2+\lambda_3^2(\eta-y)^2}\right] \\
&\quad -\frac{b_y}{2\pi Q}\left[\frac{m_{14}p_1(x-\xi)}{(x-\xi)^2+\lambda_1^2(\eta-y)^2} + \frac{m_{24}p_4(x-\xi)}{(x-\xi)^2+\lambda_2^2(\eta-y)^2} + \frac{m_{34}p_6(x-\xi)}{(x-\xi)^2+\lambda_3^2(\eta-y)^2}\right] \\
&\quad -\frac{b_{\varphi}}{2\pi Q}\left[\frac{m_{14}p_2(x-\xi)}{(x-\xi)^2+\lambda_1^2(\eta-y)^2} + \frac{m_{24}p_5(x-\xi)}{(x-\xi)^2+\lambda_2^2(\eta-y)^2} + \frac{m_{34}p_7(x-\xi)}{(x-\xi)^2+\lambda_3^2(\eta-y)^2}\right]
\end{aligned}
$$

$$
\begin{aligned}
\sigma_{xy}(x,\ y) =& \frac{b_x}{2Q'\pi}[\frac{m_{15}q_1'(x-\xi)}{(x-\xi)^2+[\lambda_1(y-\eta)]^2}+\frac{m_{25}q_2'(x-\xi)}{(x-\xi)^2+[\lambda_2(y-\eta)]^2}+\frac{m_{35}q_3'(x-\xi)}{(x-\xi)^2+[\lambda_3(y-\eta)]^2}]\\
&+\frac{b_y}{2Q\pi}[\frac{m_{15}p_1\lambda_1(y-\eta)}{(x-\xi)^2+[\lambda_1(y-\eta)]^2}+\frac{m_{25}p_4\lambda_2(y-\eta)}{(x-\xi)^2+[\lambda_2(y-\eta)]^2}+\frac{m_{35}p_6\lambda_3(y-\eta)}{(x-\xi)^2+[\lambda_3(y-\eta)]^2}]\\
&+\frac{b_\varphi}{2Q\pi}[\frac{m_{15}p_2\lambda_1(y-\eta)}{(x-\xi)^2+[\lambda_1(y-\eta)]^2}+\frac{m_{25}p_5\lambda_2(y-\eta)}{(x-\xi)^2+[\lambda_2(y-\eta)]^2}+\frac{m_{35}p_7\lambda_3(y-\eta)}{(x-\xi)^2+[\lambda_3(y-\eta)]^2}],\\
D_x(x,\ y) =& \frac{b_x}{2Q'\pi}[\frac{m_{16}q_1'(x-\xi)}{(x-\xi)^2+[\lambda_1(y-\eta)]^2}+\frac{m_{26}q_2'(x-\xi)}{(x-\xi)^2+[\lambda_2(y-\eta)]^2}+\frac{m_{36}q_3'(x-\xi)}{(x-\xi)^2+[\lambda_3(y-\eta)]^2}]\\
&+\frac{b_y}{2Q\pi}[\frac{m_{16}p_1\lambda_1(y-\eta)}{(x-\xi)^2+[\lambda_1(y-\eta)]^2}+\frac{m_{26}p_4\lambda_2(y-\eta)}{(x-\xi)^2+[\lambda_2(y-\eta)]^2}+\frac{m_{36}p_6\lambda_3(y-\eta)}{(x-\xi)^2+[\lambda_3(y-\eta)]^2}]\\
&+\frac{b_\varphi}{2Q\pi}[\frac{m_{16}p_2\lambda_1(y-\eta)}{(x-\xi)^2+[\lambda_1(y-\eta)]^2}+\frac{m_{26}p_5\lambda_2(y-\eta)}{(x-\xi)^2+[\lambda_2(y-\eta)]^2}+\frac{m_{36}p_7\lambda_3(y-\eta)}{(x-\xi)^2+[\lambda_3(y-\eta)]^2}],\\
D_y(x,y) =& \frac{b_x}{2\pi Q'}[\frac{m_{17}q_1'\lambda_1(y-\eta)}{(x-\xi)^2+\lambda_1^2(\eta-y)^2}+\frac{m_{27}q_2'\lambda_2(y-\eta)}{(x-\xi)^2+\lambda_2^2(\eta-y)^2}+\frac{m_{37}q_3'\lambda_3(y-\eta)}{(x-\xi)^2+\lambda_3^2(\eta-y)^2}]\\
&-\frac{b_y}{2\pi Q}[\frac{m_{17}p_1(x-\xi)}{(x-\xi)^2+\lambda_1^2(\eta-y)^2}+\frac{m_{27}p_4(x-\xi)}{(x-\xi)^2+\lambda_2^2(\eta-y)^2}+\frac{m_{37}p_6(x-\xi)}{(x-\xi)^2+\lambda_3^2(\eta-y)^2}]\\
&-\frac{b_\varphi}{2\pi Q}[\frac{m_{17}p_2(x-\xi)}{(x-\xi)^2+\lambda_1^2(\eta-y)^2}+\frac{m_{27}p_5(x-\xi)}{(x-\xi)^2+\lambda_2^2(\eta-y)^2}+\frac{m_{37}p_7(x-\xi)}{(x-\xi)^2+\lambda_3^2(\eta-y)^2}]
\end{aligned}
\tag{19}
$$

The solutions provided above are identical to those found in the Ref. [15].

3 Formulation of the embedded and edge cracks

Several investigators used the distributed dislocation method for modeling cracks in the elastic medium subjected to mechanical loading [26]. By employing the previously established dislocation solutions, the system of singular integral equations for a piezoelectric strip with embedded and edge cracks in a general arrangement can now be derived. The parametric representations of a crack may be expressed as:

$$x_i = x_i(s),\quad y_i = y_i(s),\quad -1 \le s \le 1,\quad i \in \{1, 2, ..., N\} \tag{20}$$

By establishing a movable local coordinate system $(t,\ n)$ with the origin positioned along the crack surface, we can express the stress and electric displacement components in these local coordinates in terms of the field components in the x–y coordinate system as follows:

$$
\begin{aligned}
\sigma_{nn} &= \frac{\sigma_{xx}+\sigma_{yy}}{2} - \frac{\sigma_{xx}-\sigma_{yy}}{2}\cos(2\psi_i) - \sigma_{xy}\sin(2\psi_i),\\
\sigma_{nt} &= -\frac{\sigma_{xx}-\sigma_{yy}}{2}\sin(2\psi_i) + \sigma_{xy}\cos(2\psi_i),\\
D_n &= D_y\cos(\psi_i) - D_x\sin(\psi_i).
\end{aligned}
\tag{21}
$$

The relationship between the components of the Burgers vectors in the two previously mentioned coordinate systems is as follows:

$$\begin{Bmatrix} b_x \\ b_y \end{Bmatrix} = \begin{bmatrix} \cos(\psi_j) & -\sin(\psi_j) \\ \sin(\psi_j) & \cos(\psi_j) \end{bmatrix} \begin{Bmatrix} b_t \\ b_n \end{Bmatrix} \tag{22}$$

where $\psi_k(t) = \tan^{-1}(y_k'(t)/x_k'(t)),\quad k = i,\ j$ is the angle between t- and x-axes. By applying Bueckner's principle and integrating over the crack surface, we derive three Cauchy singular integral equations for multiple interacting impermeable embedded and edge cracks.

$$\begin{Bmatrix} \sigma_{nni}(x_k(s), y_k(s)) \\ \sigma_{nti}(x_k(s), y_k(s)) \\ D_{ni}(x_k(s), y_k(s)) \end{Bmatrix} = \sum_{k=1}^{N} \int_{-1}^{1} \begin{bmatrix} K_{11ik}(s,p) & K_{12ik}(s,p) & K_{13ik}(s,p) \\ K_{21ik}(s,p) & K_{22ik}(s,p) & K_{23ik}(s,p) \\ K_{31ik}(s,p) & K_{32ik}(s,p) & K_{33ik}(s,p) \end{bmatrix} \begin{Bmatrix} B_{tk}(p) \\ B_{nk}(p) \\ B_{\varphi k}(p) \end{Bmatrix} dp, \quad -1 \le s \le 1. \tag{23}$$

The kernels in Eq. (23) can be found in Ref. [15]. For an embedded crack, we note that the following closure relations should complement Cauchy singular integral Eqs. (23):

$$\left\{\begin{array}{c} u_{ti}^{+}(s)-u_{ti}^{-}(s) \\ u_{ni}^{+}(s)-u_{ni}^{-}(s) \\ \varphi_{i}^{+}(s)-\varphi_{i}^{-}(s) \end{array}\right\}=\int_{-1}^{s}\left\{\begin{array}{c} b_{ti}(p) \\ b_{ni}(p) \\ b_{\varphi i}(p) \end{array}\right\} L_i(p) dp=0 \quad i \in\{1,2,\ldots,N\}, \quad -1 \leq p \leq 1. \tag{24}$$

where $L_i(p)=\sqrt{\left[\alpha_i'(p)\right]^2+\left[\beta_i'(p)\right]^2}$. The unknown dislocation densities on the crack surface are determined by solving the system of singular integral equations in Eq. (21), taking into account the conditions specified in Eq. (24). The solution of singular integral equations is accomplished numerically by using the technique rendered by Faal et al. [27]. Due to the singularity of the field components near a crack tip, the unknown functions associated with an embedded crack are considered as follows:

$$B_{ki}(p)=\frac{g_{ki}(p)}{\sqrt{1-p^2}} \quad -1 \leq p \leq 1, \quad k \in\{n, t, \varphi\}. \tag{25}$$

and for the edge crack, it is represented by

$$B_{ki}(p)=g_{ki}(p) \sqrt{\frac{1-p}{1+p}} \quad -1 \leq p \leq 1, \quad k \in\{n, t, \varphi\}. \tag{26}$$

The modes I, II stress and displacement intensity factors are defined as follows:

$$\begin{aligned}
K_{IR} &= \lim_{r \to 0} \sqrt{2r}\,\sigma_n(r, 0), \\
K_{IL} &= \lim_{r \to 0} \sqrt{2r}\,\sigma_n(r, \pi), \\
K_{IIR} &= \lim_{r \to 0} \sqrt{2r}\,\sigma_s(r, 0), \\
K_{IIL} &= \lim_{r \to 0} \sqrt{2r}\,\sigma_s(r, \pi), \\
K_{DR} &= \lim_{r \to 0} \sqrt{2r}\,D_n(r, 0), \\
K_{DL} &= \lim_{r \to 0} \sqrt{2r}\,D_n(r, \pi).
\end{aligned} \tag{30}$$

where the right and left crack tips of the crack are defined by subscripts R and L, respectively. It is easy to show that, for $i=k$ as $p \rightarrow s$, the kernels in Eq. (23) have Cauchy-type singularity. To extract the singular terms the Taylor series expansion of $x_i(p)$ and $y_i=y_i(p)$ in the vicinity of s is plugged into the kernels of integral Eqs. (23), then we have:

$$K_{klii}(s, p)=\frac{f_{kl,-1i}(s)}{s-p}+\sum_{m=0}^{\infty} f_{kl,mi}(s)(s-p)^m, \quad k, l \in\{1,2,3\}. \tag{31}$$

The coefficients of singular terms are identical to those obtained for the piezoelectric plane by Mahmoudi and Ayatollahi [15]. Substituting Eqs. (31), (25), and (26) into Eq. (23), and then substituting the resulting equations into Eq. (31), yields the field intensity factors at the crack tips $s=\pm 1$ for the i^{th} crack:

$$\begin{aligned}
\left\{\begin{array}{c} K_{IRi} \\ K_{ILi} \end{array}\right\} &= \pm \pi \sqrt{L_{\pm}}\left[f_{11,-1i}(\pm 1) g_{si}(\pm 1)+f_{12,-1i}(\pm 1) g_{ni}(\pm 1)+f_{13,-1i}(\pm 1) g_{\varphi i}(\pm 1)\right], \\
\left\{\begin{array}{c} K_{IIRi} \\ K_{IILi} \end{array}\right\} &= \pm \pi \sqrt{L_{\pm}}\left[f_{21,-1i}(\pm 1) g_{si}(\pm 1)+f_{22,-1i}(\pm 1) g_{ni}(\pm 1)+f_{23,-1i}(\pm 1) g_{\varphi i}(\pm 1)\right], \\
\left\{\begin{array}{c} K_{DRi} \\ K_{DLi} \end{array}\right\} &= \pm \pi \sqrt{L_{\pm}}\left[f_{31,-1i}(\pm 1) g_{si}(\pm 1)+f_{32,-1i}(\pm 1) g_{ni}(\pm 1)+f_{33,-1i}(\pm 1) g_{\varphi i}(\pm 1)\right], \quad i \in\{1,2, N\}.
\end{aligned} \tag{32}$$

where $L_{\pm}=\left([\alpha_i'(\pm 1)]^2+[\beta_i'(\pm 1)]^2\right)^{\frac{1}{2}}$.

4 Results and discussion

First, the validity of the formulation is examined, and the effectiveness of the proposed methodology is demonstrated through several examples. The validity of the procedure is confirmed by reducing the problem to an infinite piezoelectric layer with an embedded crack of varying orientations (Fig. 1a). The results show excellent agreement with those reported by Bagheri et al. [18].

Furthermore, as an additional verification, the formulation is validated by analyzing an infinite piezoelectric plane containing two interacting parallel cracks. Figures 1b,c illustrate the variations of the non-dimensional mode I stress intensity factors with crack location under different electrical loading conditions. The plots show excellent agreement with those obtained by Monfared and Ayatollahi [15].

A divisor $K_0 = \sigma_0\sqrt{l}$ is the stress intensity factor of an embedded crack in an infinite elastic plane, in which σ_0 represents the applied traction and l half of the crack length. Additionally, the electric intensity factor is normalized by $K_{0D} = \sigma_0 e_{15}\sqrt{l}\big/ c_{44}$. In the sequel, unless stated otherwise, the electro-mechanical loading parameter factor will be assumed to be as $\lambda_D = 1$, which is defined by $\lambda_D = e_{15}D_0\big/\sigma_0\varepsilon_{11}$. It is worth mentioning that the loading parameter is influenced by both the normal traction σ_0 and electrical loading D_0. The piezoelectric layer is composed of Cadmium Selenide with the following engineering constants [28]:

$$\begin{aligned}
&c_{11} = 7.41\times 10^{10}(\frac{N}{m^2}),\ c_{33} = 8.36\times 10^{10}(\frac{N}{m^2}),\ c_{44} = 1.32\times 10^{10}(\frac{N}{m^2}),\ c_{13} = 3.93\times 10^{10}(\frac{N}{m^2})\\
&e_{31} = -0.16(\frac{C}{m^2}),\ e_{33} = 0.347(\frac{C}{m^2}),\ e_{15} = -0.138(\frac{C}{m^2}), \varepsilon_{11} = 0.825\times 10^{-10}(\frac{C}{Vm}),\\
&\varepsilon_{33} = 0.903\times 10^{-10}(\frac{C}{Vm}),
\end{aligned} \tag{33}$$

It is important to emphasize that this study does not address crack closure. Therefore, in all examples, both the loading conditions and the defect configuration must be designed to prevent any possibility of cracks closing.

4.1 Single crack problems

Figures 2b-d and 4b-d show the variation of modes I, II stress, and electric displacement intensity factors as the crack inclination angle changes, ψ. The first problem is a fixed-centered embedded crack, located at (0, $h\big/2$) while its orientation is changing. The crack with length $l\big/h = 0.3$, subjected to constant traction and electric displacement, $\sigma_{yy} = \sigma_0$ and $D_y = D_0$, on the edges. The problem exhibits symmetry about the y-axis; consequently, the stress intensity factors at both crack tips, R and L, are identical. The crack at the horizontal position experiences only opening, resulting in a maximum mode I stress intensity factor (Fig. 2b). The mode II stress intensity factors are zero because the shear traction on the crack has vanished. (Fig. 2c). As expected, the mode I stress intensity factor decreases with increasing crack orientation angle. For an inclined crack, the applied constant traction can be resolved into two components relative to the crack plane: a normal component and a tangential (shear) component. The normal traction component drives Mode I (opening mode) fracture by contributing to the Mode I stress intensity factor K_I, whereas the tangential component induces in-plane shear, thereby contributing to the Mode II stress intensity factor K_{II}. As the crack orientation angle increases from 0 to 90°, the normal component of the applied traction diminishes, leading to a corresponding reduction in the Mode I stress intensity factor K_I.The results show that the mode-II stress intensity factor increases with the crack orientation angle, reaching a maximum before monotonically decreasing to a minimum value. The stress intensity factor is at its minimum for a crack positioned vertically because the shear traction on the crack surface is zero. It is essential to note that the effects of the electromechanical loading parameter on Mode I and Mode II stress intensity factors are negligible for both horizontal and vertical cracks. However, for oblique cracks, the influence of λ_D on stress intensity is more pronounced. To further elucidate this effect, a comparison between Fig. 2b and c reveal that, for most crack orientation angles, increasing λ_D from a negative to a positive value results in an increase in the Mode I stress intensity factor K_I, while simultaneously reducing the Mode II stress intensity factor K_{II}. It is well recognized that the application of an electric field can modulate the influence of mechanical loading. To gain deeper insight into the electromechanical coupling behavior, we analyze the effect of crack inclination on the electric displacement intensity factor along the crack front.

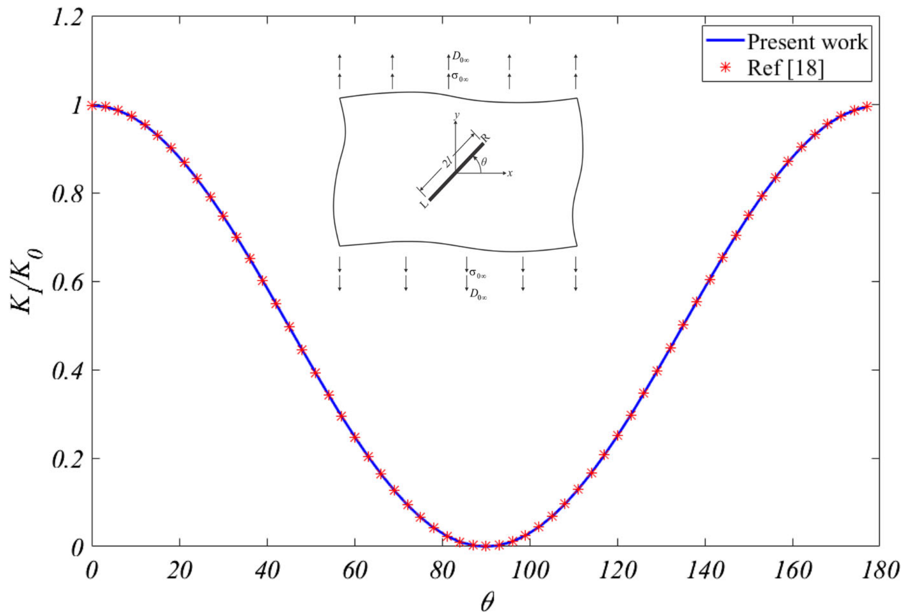

(a)

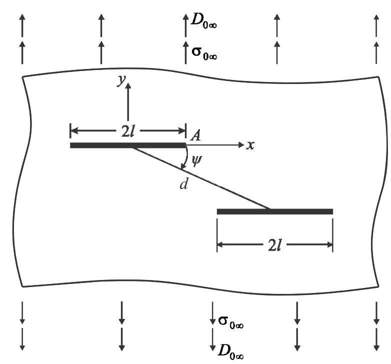

(b)

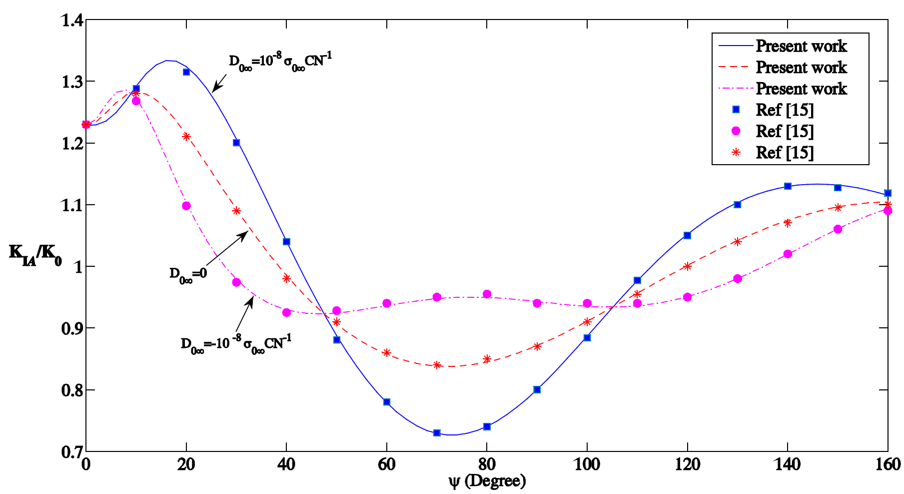

(c)

Fig. 1 **a.** Variation of mode I stress intensity factors of a single crack in an infinite plane. **b.** Piezoelectric plane weakened by two parallel crackscracks.**c.** Variation of mode I stress intensity factors of two parallel cracks for $d/l = 2.5$

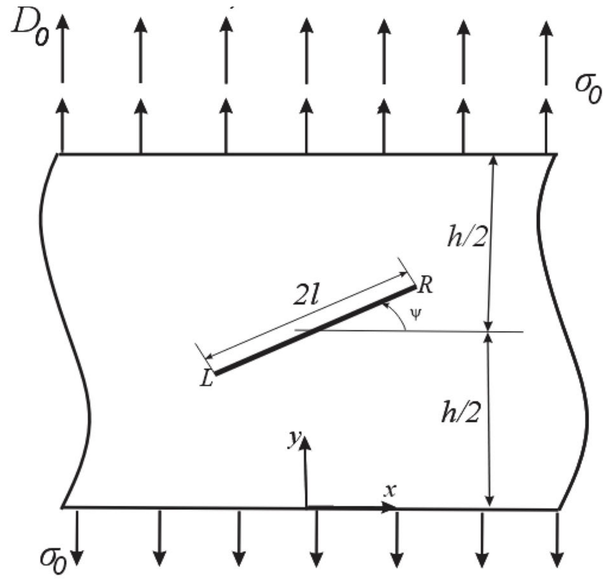

(a)

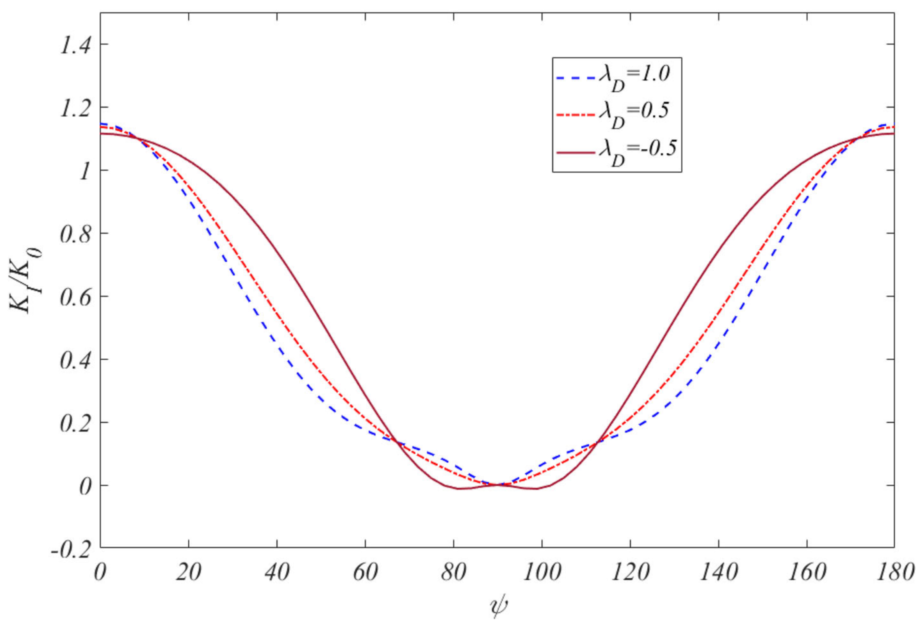

(b)

Fig. 2 **a.** piezoelectric strip with embedded crack. **b.** Variation of mode I stress intensity factors of an embedded crack with different orientations. **c.** Variation of mode II stress intensity factors of a crack with different orientations. **d.** Variation of electric displacement intensity factors of a crack with different orientations

Figure 2d illustrates how crack inclination affects the electric displacement intensity factor across various values of the loading parameter. It is important to note that, for horizontal cracks, the effect of λ_D on electric displacement intensity factor is the largest. As illustrated in Fig. 2d, for decreasing values of the positive λ_D, the variation of the electric displacement intensity factor with respect to crack inclination diminishes. This behavior is attributed to the impermeable nature of the crack faces, which act as barriers to the electric field, thereby impeding its transmission across the crack front. When the crack is not oriented perpendicular to the direction of the electric field, its obstructive effect weakens, resulting in a reduction of the electric displacement

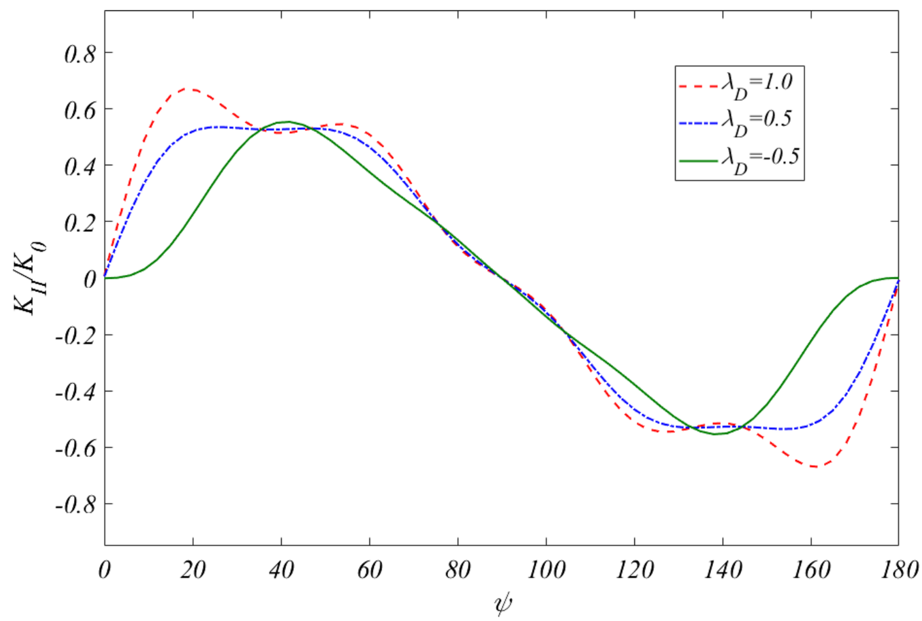

(c)

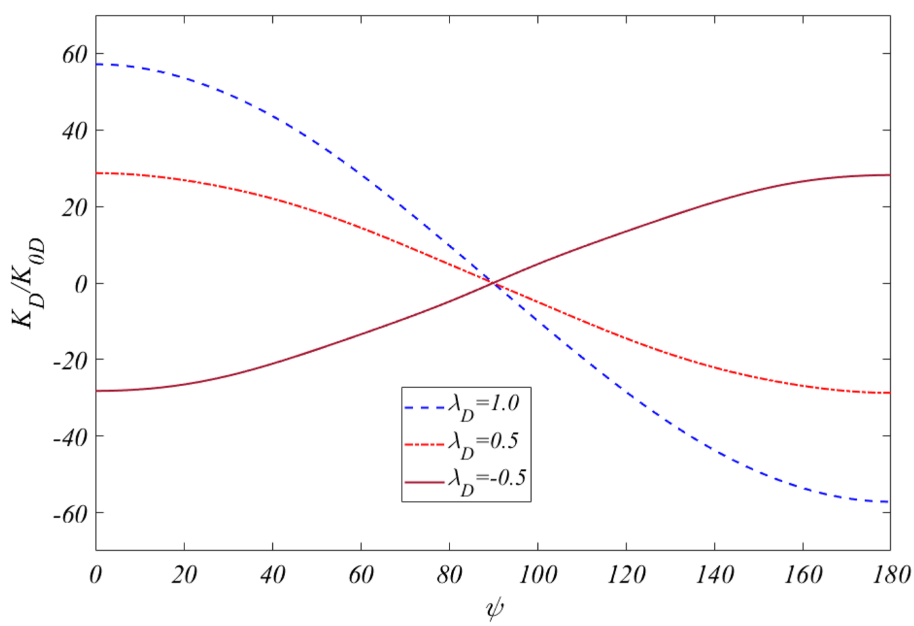

(d)

Fig. 2 continued

intensity factor. In essence, the crack inclination governs both the relative magnitudes of the normal and shear tractions and the extent to which the impermeable crack impedes the electric field.

In the following example, we examine a horizontal crack by varying its length, which is located at different distances from the boundary of the piezoelectric strip (Fig. 3a-c). The plots of the field intensity factors versus normalized crack length are presented in Fig. 3a-c. For the Mode I stress intensity factor, the boundary effect is minimal, and the behavior of the crack resembles that of a crack in an infinite plane. This is because mechanical loading applied farther from the crack tip results in reduced crack opening, thereby leading to a lower Mode I stress intensity factor. It has been found that the location of the crack significantly affects the Mode II stress intensity factor and the electric displacement intensity factor.

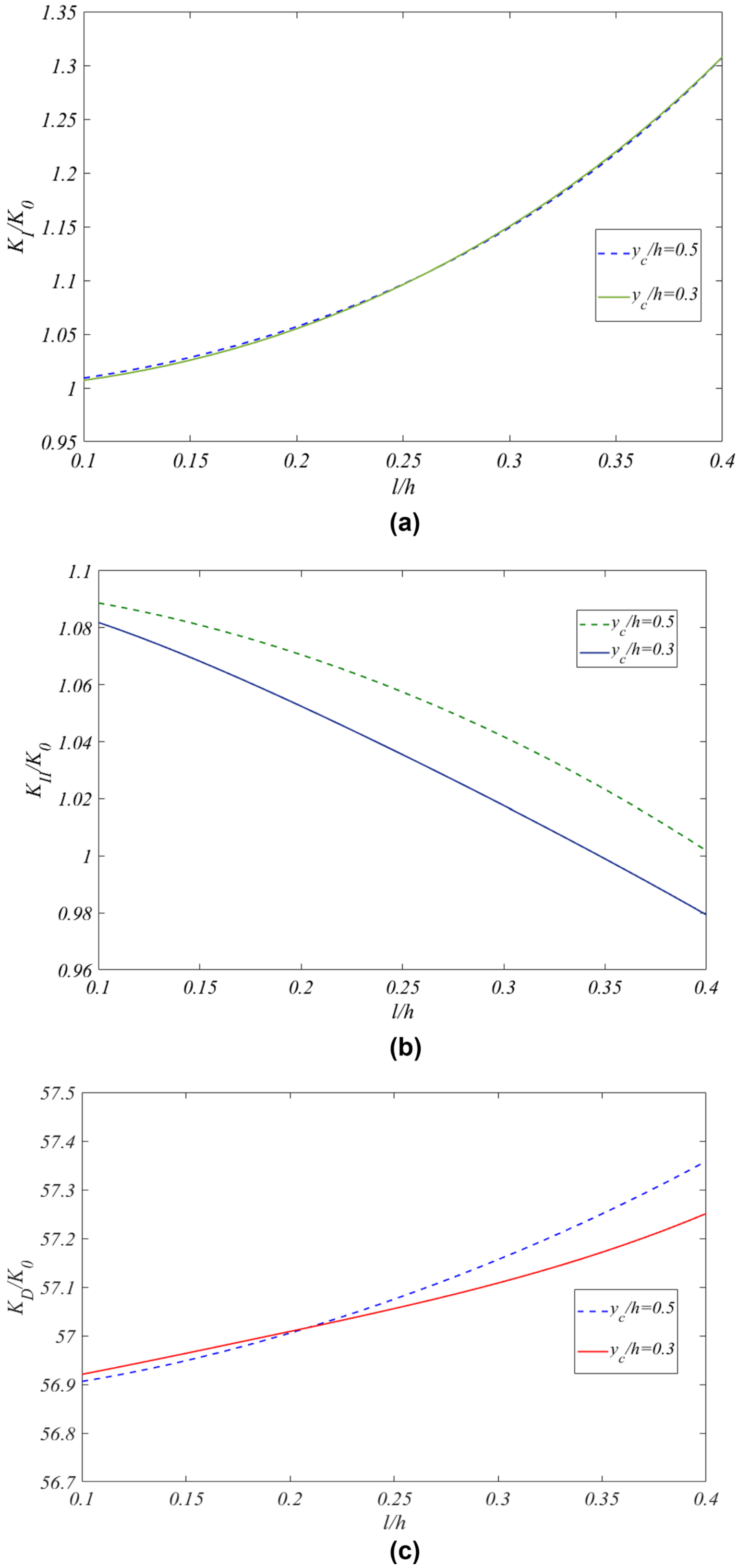

Fig. 3 **a.** Variation of mode I stress intensity factors of an embedded crack with crack length at different locations. **b.** Variation of mode II stress intensity factors of an embedded crack with crack length at different locations. **c.** Variation of electric displacement intensity factors of an embedded crack with crack length at different locations

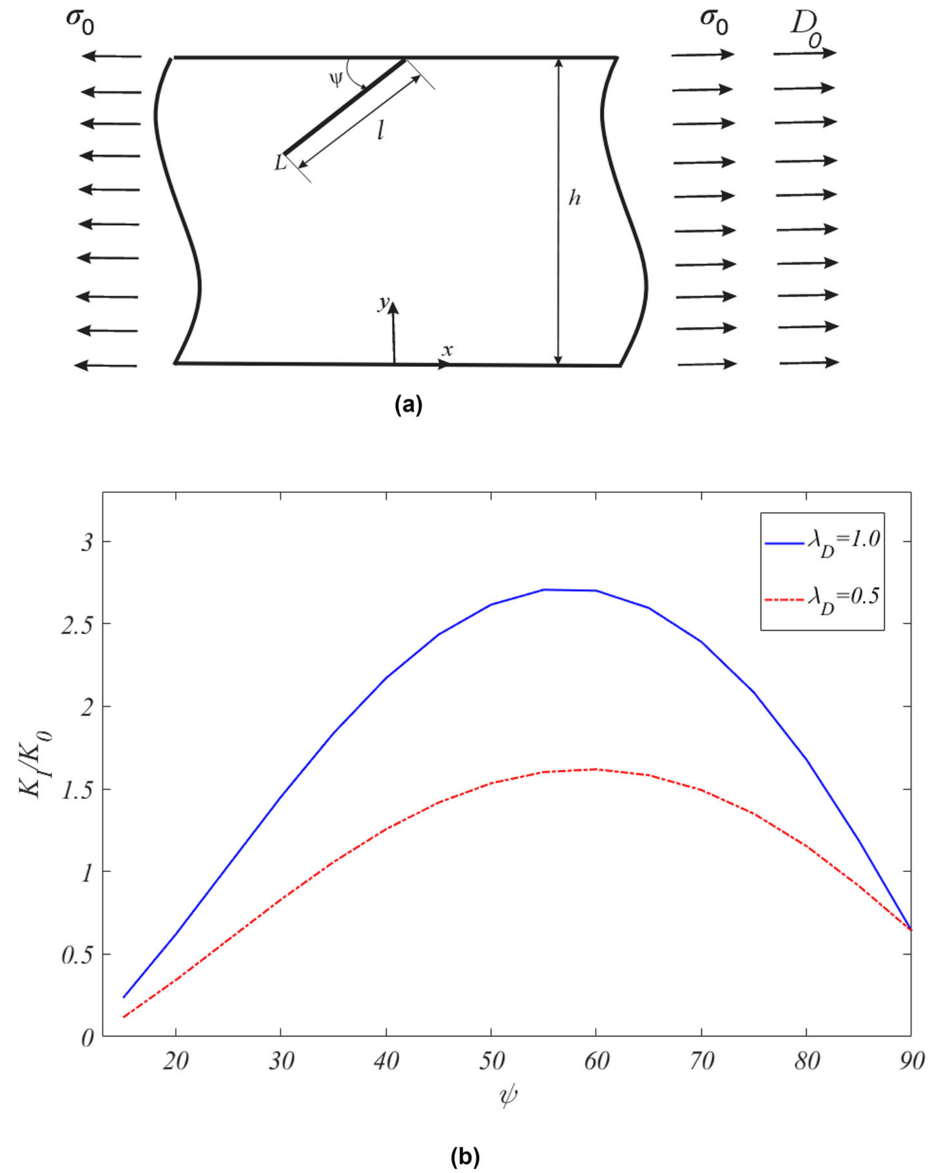

Fig. 4 **a.** Piezoelectric strip with edge crack. **b.** Variation of mode I stress intensity factors of an edge crack with different orientations. **c.** Variation of mode II stress intensity factors of an edge crack with different orientations. **d.** Variation of electric displacement intensity factors of an edge crack with different orientations

In continuation of the previous example, an oblique edge crack is considered similar to the first example, as illustrated in Fig. 4a. To facilitate crack opening, we subject the strip to normal traction $\sigma_{xx} = \sigma_0$ and electric displacement $D_x = D_0$. Additionally, the crack angle falls within the range where the crack opening occurs. The analysis focuses on an edge crack under various loading parameters λ_D. Figure 4b-d depict variations of field intensity factors versus crack orientation ψ. As shown in the figures, the influence of the magnitude and sign of the electromechanical loading parameter on Modes I and II is more pronounced than that of the embedded crack. As observed in Fig. 4d, when the crack is not oriented perpendicular to the electric field direction, the impermeable crack acts as a less effective barrier, resulting in a decreased electric displacement intensity factor.

The variations of mode I and mode II stress intensity factors, as well as the electric displacement factor of an edge crack with varying crack lengths at different orientations, are displayed in Fig. 5a-c. Comparing the mode I stress intensity factor reveals that the vertical edge crack has a different trend, which is observed at $\psi = \pi/2$. The mode I stress intensity factor decreases by increasing the crack length, whereas the reverse

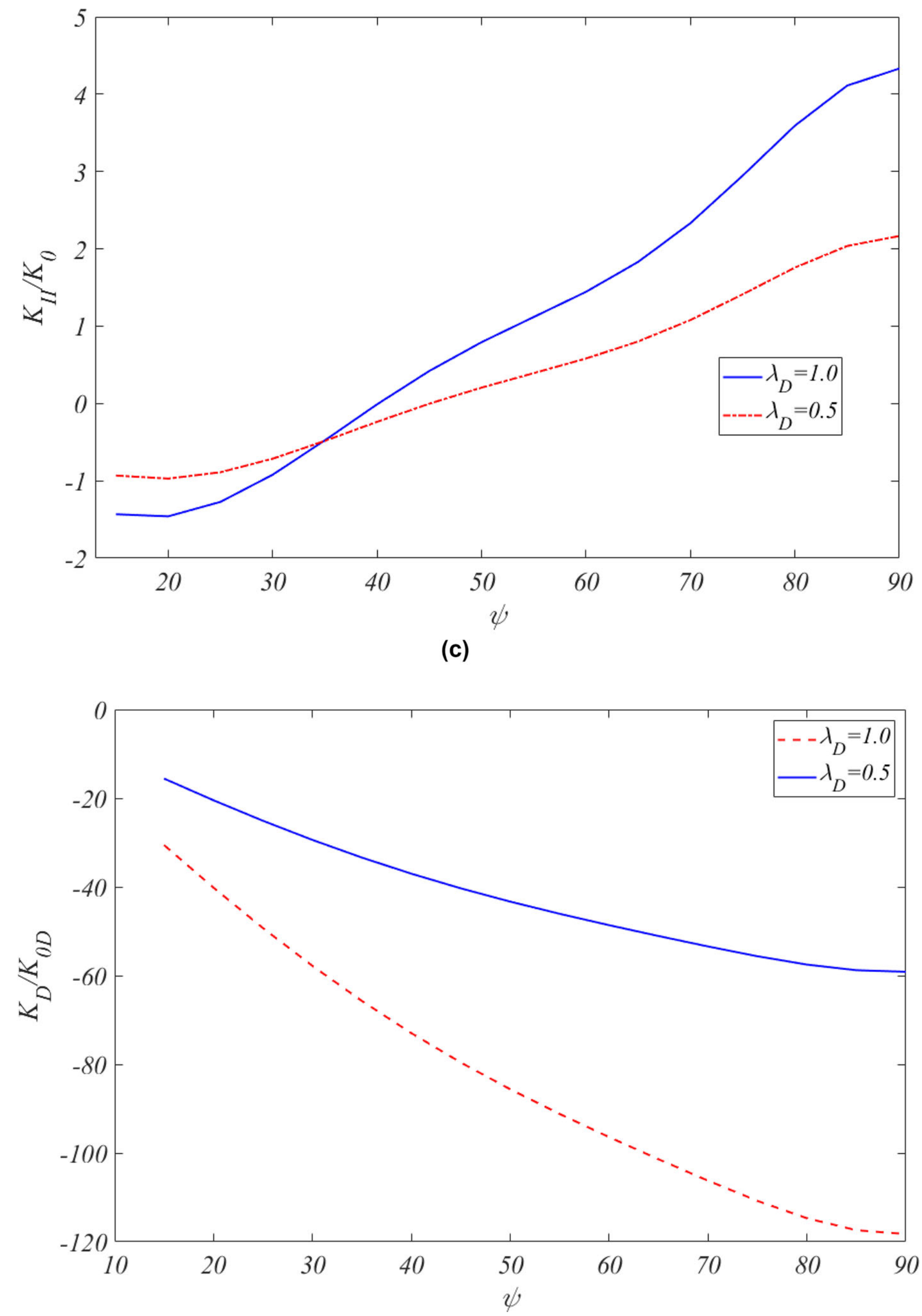

Fig. 4 continued

holds for mode II and electric displacement factor. The mode II stress intensity factor of the inclined crack increases with increasing crack orientation angle ψ. The underlying reason for these behaviors is that the normal component of the mechanical loading relative to the crack face, governed by the crack orientation angle, plays a more significant role than the crack length.

4.2 Two interacting embedded and edge crack

This methodology is applied to address several new problems, demonstrating its effectiveness. The interaction of two identical embedded cracks under biaxial mechanical loadings and electrical loading $D_y = D_0$ is shown

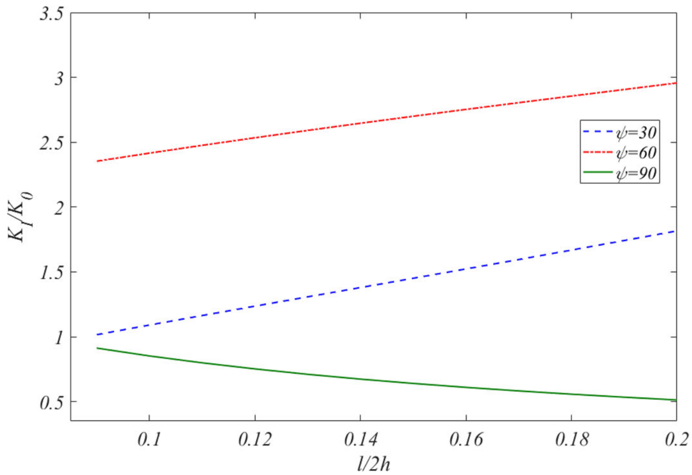

(a)

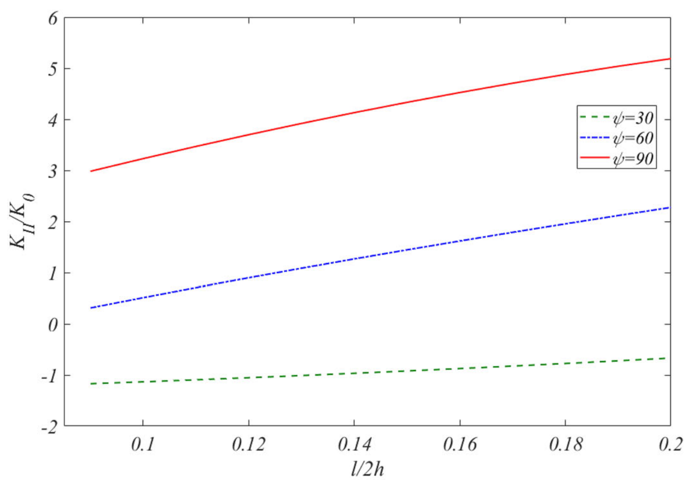

(b)

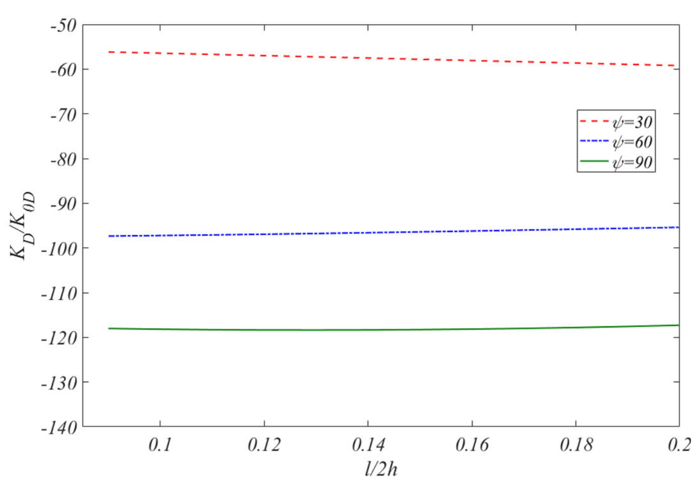

(c)

Fig. 5 **a.** Variation of mode I stress intensity factors of an edge crack with crack length at different orientations. **b.** Variation of mode II stress intensity factors of an edge crack with crack length at different orientations. **c.** Variation of electric displacement intensity factors of an edge crack with crack length at different orientations

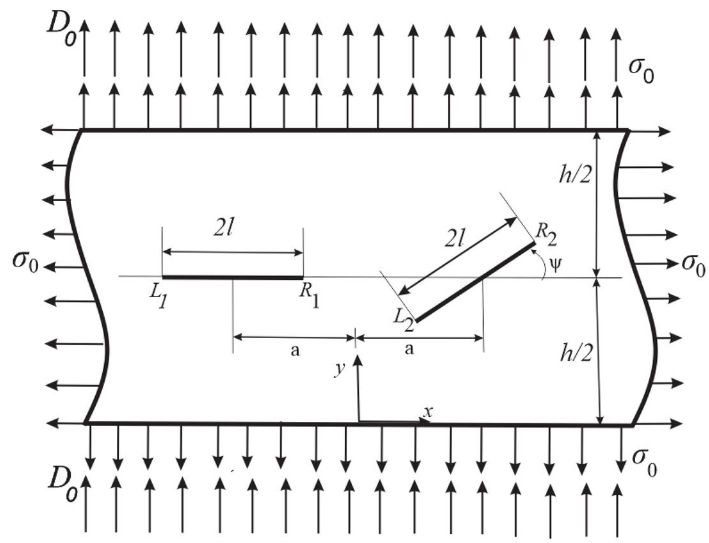

(a)

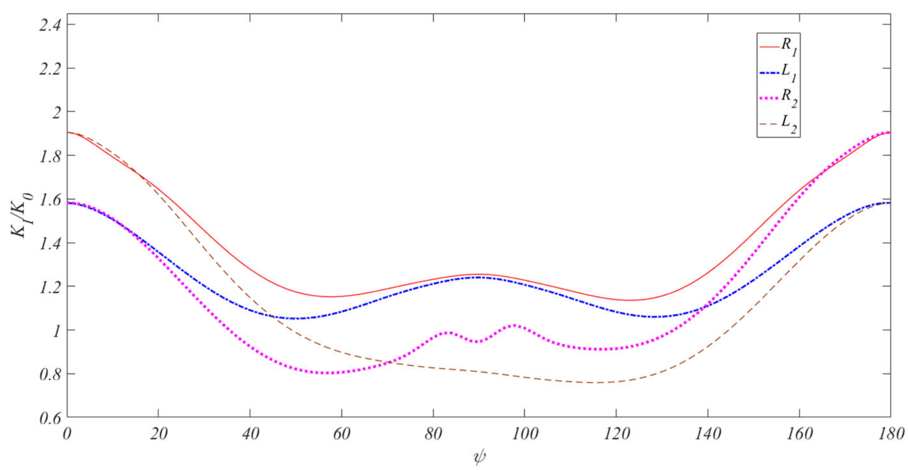

(b)

Fig. 6 **a.** Piezoelectric strip with two interacting embedded cracks. **b.** Variation of Mode I stress-intensity factor for a stationary and rotating crack. **c.** Variation of Mode II stress-intensity factor for a stationary and rotating crack. **d.** Variation of electric displacement intensity factor for a stationary and rotating crack

in Fig. 6a. The distance between the centers of the cracks is fixed, while the orientation of the crack $\boldsymbol{L_2R_2}$ is changing. As it is expected, the highest K_I/K_0 occurs in the case of coaxial cracks, i.e., $\psi = 0$. The variations in field intensity factors at all crack tips are significant due to the changing orientations of the cracks, as well as the varying traction and interactions occurring simultaneously (Fig. 6b). The mode II stress-intensity factor for tip $\boldsymbol{L_1}$ and $\boldsymbol{R_1}$ vanishes at $\psi = 0$ and $\psi = \pi/2$ which is due to the symmetry concerning the x-axis. Moreover, the range of variations of the mode II stress intensity factor of interacting tips is extensive compared to the other tips of cracks (Fig. 6c).

Two cracks are considered in this analysis: an edge crack with a length of $l/h = 0.3$ and a rotating embedded crack with a length of $l/h = 0.3$. Figures 7a - c depict the dimensionless modes I and II stress-intensity factors, as well as the electric displacement intensity factor against the orientation of the embedded crack, where the center of the crack is fixed. To ensure that the cracks open in any configuration, the piezoelectric strip is under constant mechanical biaxial tractions and electric displacement $D_y = D_0$ on the edges and at the far-field, $|x| \to \infty$. From Figs. 7a - c, we may conclude that the crack inclination angle dominates the intensity of stress and electric displacement distributions in a piezoelectric strip, causing higher field intensity

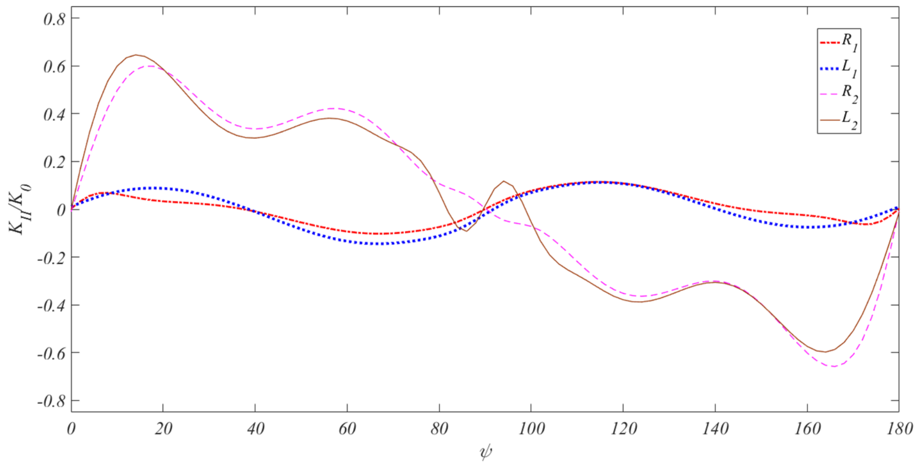

(c)

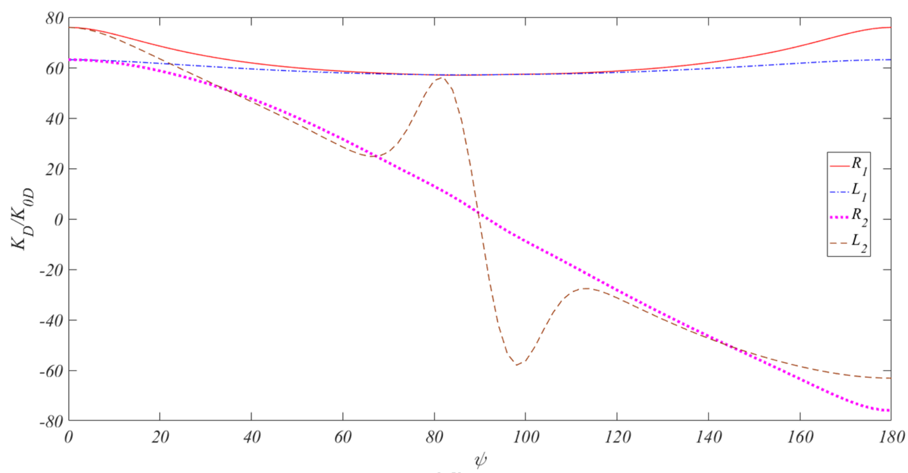

(d)

Fig. 6 continued

factors. The effect of embedded crack orientations on the electric displacement intensity factor is minimal for $\psi < 30$, but for $\psi > 30$, significant variations are observed in Fig. 7d. In this example, the rotation of the embedded crack alters the distance between the interacting crack tips, which significantly influences the stress intensity factors at the crack tips. As a final example, we examine the interaction between edge cracks and embedded cracks of varying lengths (Fig. 8a). Figure 8b–d present the variations of the mode I and mode II stress intensity factors, along with the electric displacement factor, as functions of l_1 / h. The length of the edge crack is fixed $l_2 / h = 0.3$, whereas the length of the crack $L_1 R_1$ changes in the direction of the centerline of the layer for $a / h = 0.4$. As expected, the interaction between the cracks amplifies the mode I and mode II stress intensity factors, with the effect being more pronounced at R_1, due to its proximity to the adjacent crack.

5 Concluding remarks

Piezoelectric layers are key enablers in smart sensing, energy-efficient actuation, and autonomous systems. Their integration into multifunctional materials and devices supports advancements in aerospace, civil infrastructure, medical technology, and wearable electronics. The theoretical solution for a piezoelectric strip under mixed-mode conditions, containing several edge and embedded cracks, was addressed using the distributed dislocation technique. The stresses and electric displacements at the dislocation location show the traditional Cauchy singularities. The method facilitates the simultaneous modeling of embedded and edge cracks within the piezoelectric strip under mixed-mode conditions. The numerical results lead to the following conclusions:

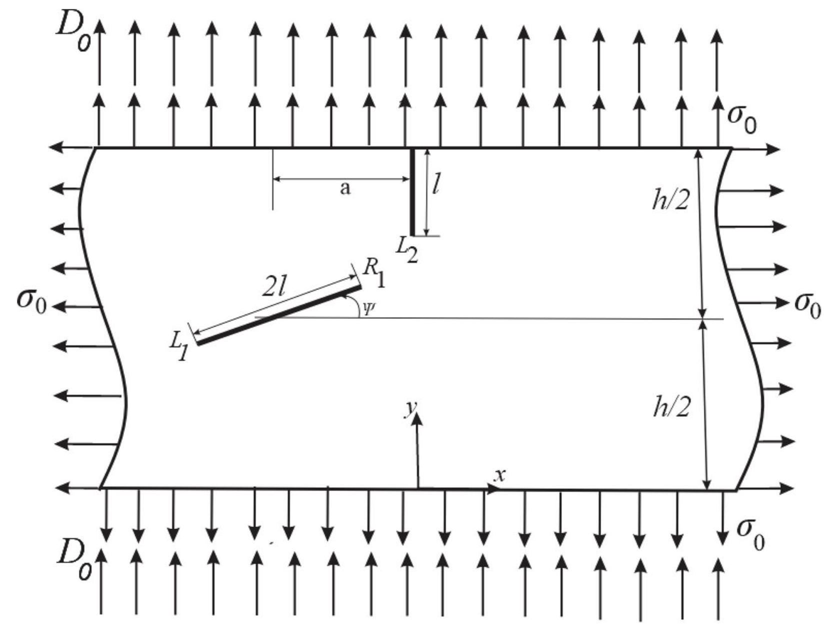

(a)

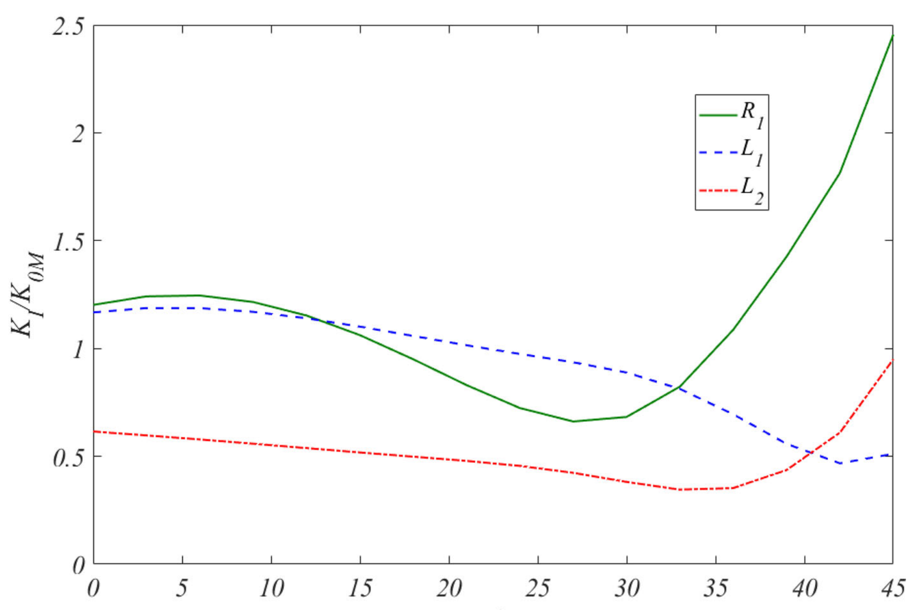

(b)

Fig. 7 **a.** Piezoelectric strip with two interacting embedded and edge cracks. **b.** Variation of Mode I stress-intensity factor for an edge and a rotating embedded crack. **c.** Variation of Mode II stress-intensity factor for an edge and a rotating embedded crack. **d.** Variation of electric displacement intensity factor for an edge and a rotating embedded crack

Remark 1 The formulation can analyze several edge and embedded cracks.

Remark 2 Crack orientation significantly affects the stress intensity factors of modes I and II, as well as the electric displacement factors.

Remark 3 The field intensities increase with an increase in crack length. For a crack oriented parallel to the strip boundaries, the crack position significantly affects Mode II stress intensity factors and electric displacement factors, while it has a negligible impact on Mode I stress intensity factors.

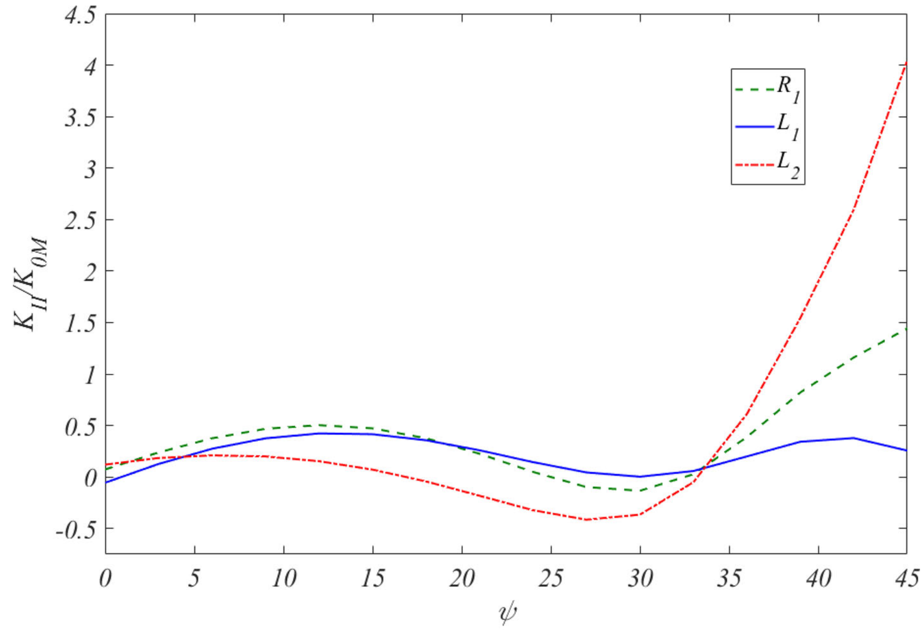

(c)

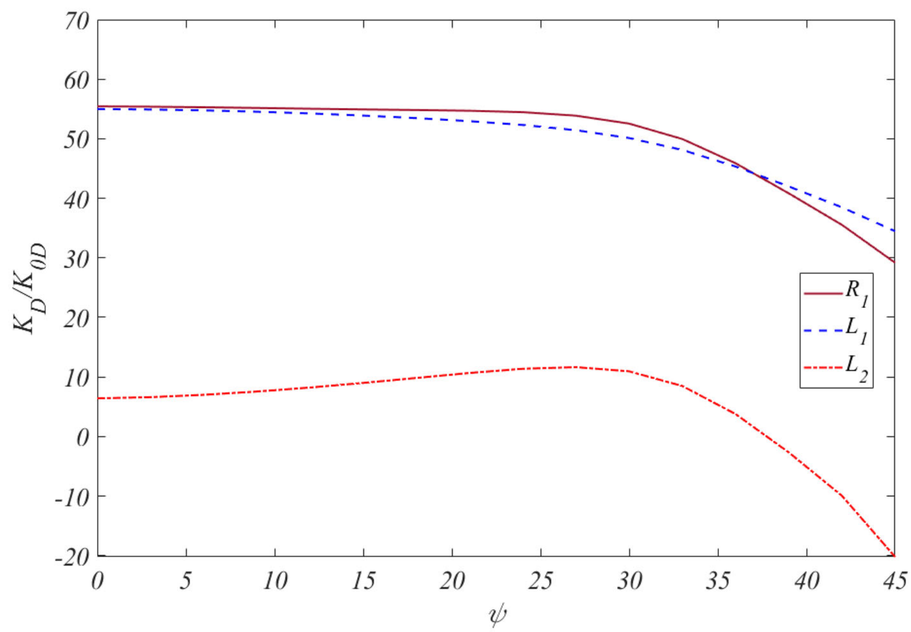

(d)

Fig. 7 continued

Remark 4 The result of the edge crack reveals that the loading parameter significantly influences the field intensity factors at the crack tip.

Remark 5 The study indicates that there are some special orientations at which the increase of the crack length does not influence the mode I stress intensity factor of an edge crack.

Remark 6 The variations in the field intensity factors for two interacting cracks depend on the location and orientation of the rotating crack.

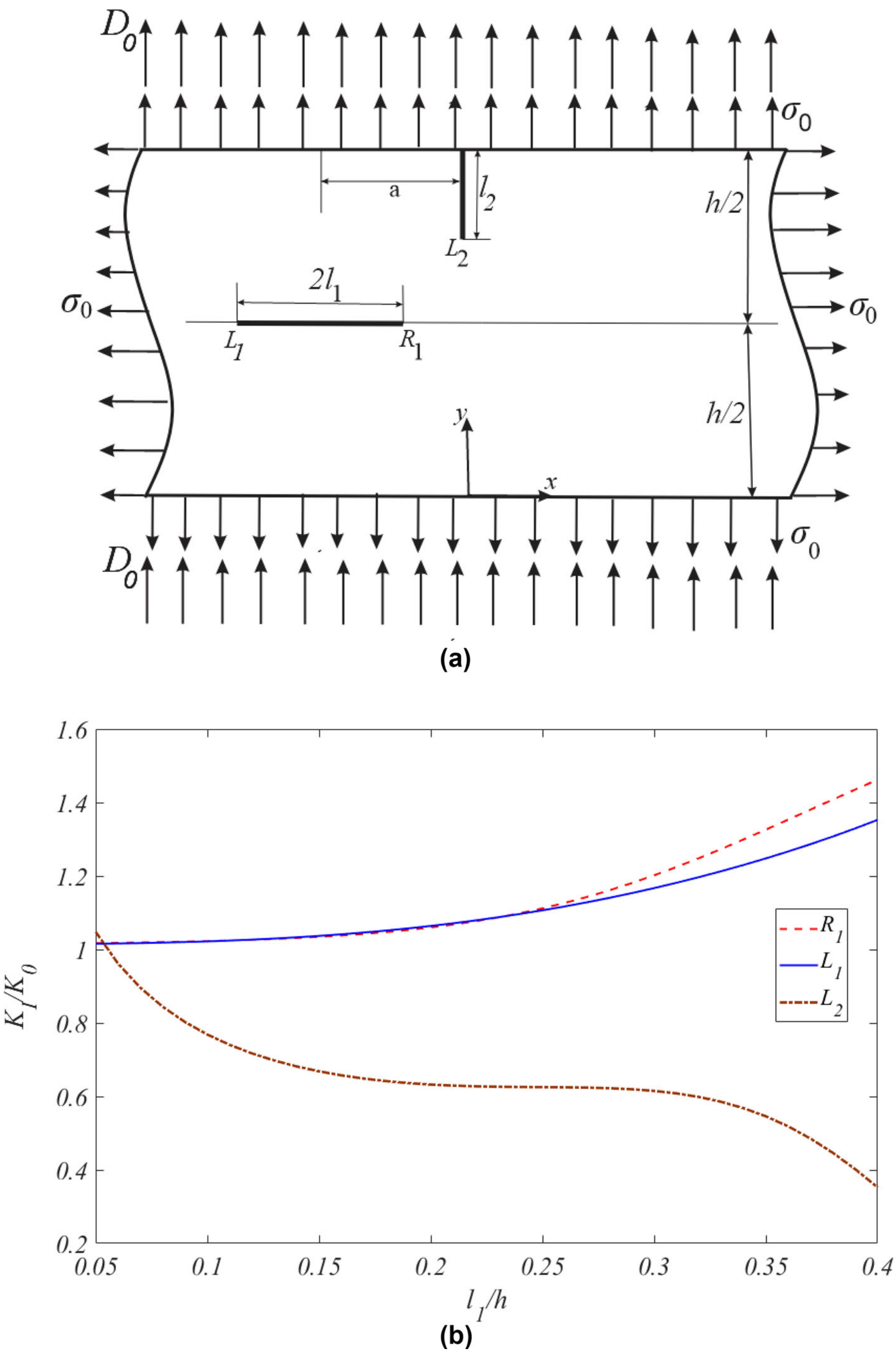

Fig. 8 **a.** Piezoelectric strip with two interacting horizontal embedded and vertical edge cracks. **b.** Variation of Mode I stress-intensity factor of an edge and a horizontal embedded crack with different lengths.**c.** Variation of Mode II stress-intensity factor of an edge and a horizontal embedded crack with different lengths. **d.** Variation of electric displacement intensity factor of an edge and a horizontal embedded crack with different lengths

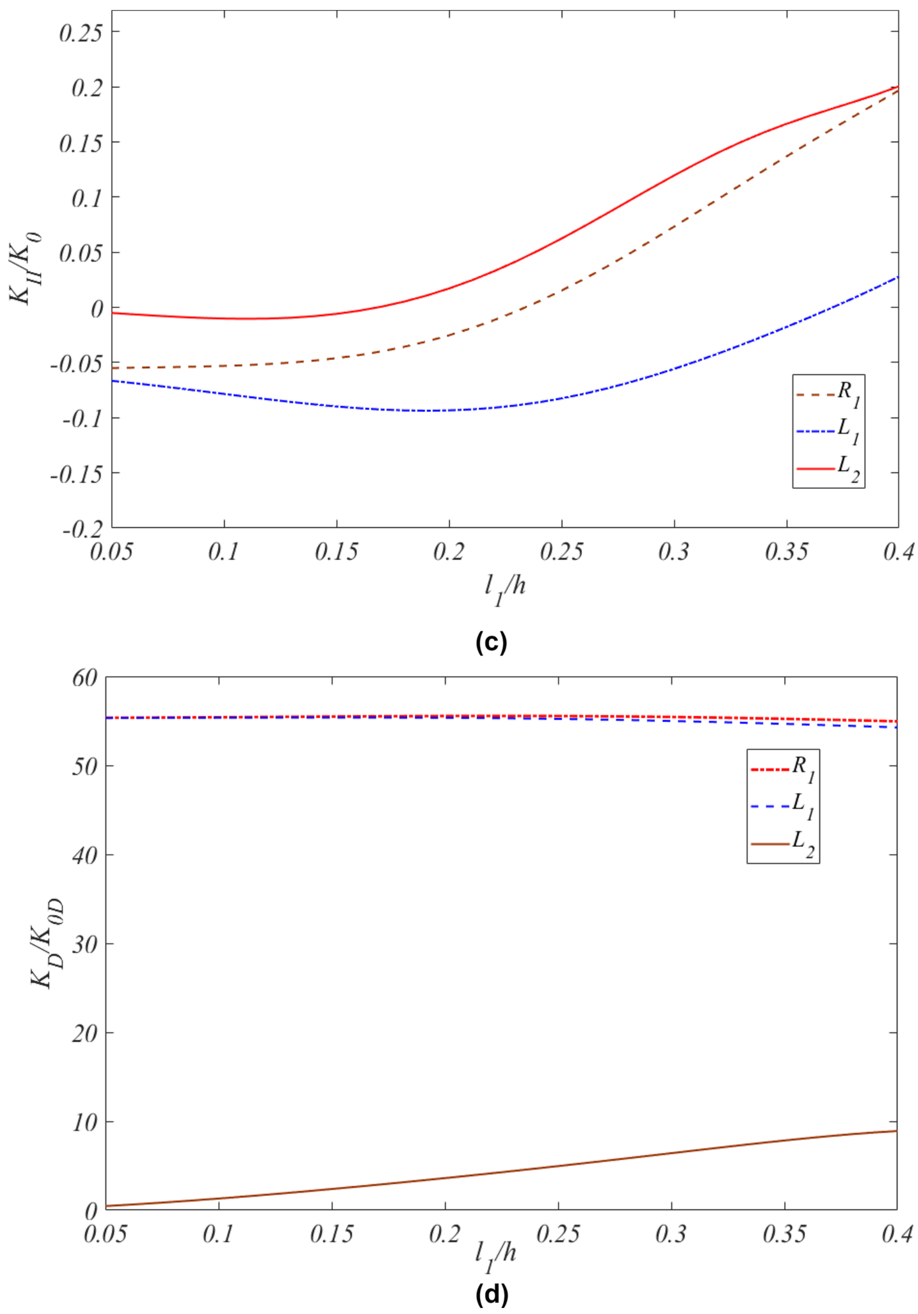

Fig. 8 continued

Remark 7 A key limitation of the present formulation is the exclusion of crack-face contact phenomena. Consequently, the applied tractions must be restricted to conditions that prevent any partial or complete closure of the crack surfaces.

Remark 8 As future work, the analysis can be extended to include piezoelectric materials with nonlinear behavior by employing mathematical tools reported in the literature [29–31]. This approach allows for a more accurate representation of the material response under high electric fields and complex loading conditions, offering a more realistic framework for fracture analysis.

Funding No funding.

Conflict of Interest We declare that there is no conflict of interest between the authors.

Appendix

The coefficients in (11) are:

$$
\begin{aligned}
m_{j3} &= c_{11} + c_{13}\lambda_j m_{j1} + e_{31}\lambda_j m_{j2} \\
m_{j4} &= c_{13} + c_{33}\lambda_j m_{j1} + e_{33}\lambda_j m_{j2} \\
m_{j5} &= -c_{44}\lambda_j + c_{44} m_{j1} + e_{15} m_{j2} \\
m_{j6} &= -e_{15}\lambda_j + e_{15} m_{j1} - \varepsilon_{11} m_{j2} \\
m_{j7} &= e_{31} + e_{33}\lambda_j m_{j1} - \varepsilon_{33}\lambda_j m_{j2}
\end{aligned} \tag{A.1}
$$

The coefficients in Eq. (12) are**:**

$$
\begin{aligned}
E_{11x} &= \frac{1}{2Q'D}\{E_1 q_1' e^{s\lambda_1\eta} + 2E_2 q_2' e^{s\lambda_2\eta} + 2E_3 q_3' e^{s\lambda_3\eta} + E_4 q_1' e^{-s\lambda_1\eta} + 2E_5 q_2' e^{-s\lambda_2\eta} + 2E_6 q_3' e^{-s\lambda_3\eta}\} \\
E_{11y} &= -\frac{1}{2QD}\{E_1 p_1 e^{s\lambda_1\eta} + 2E_2 p_4 e^{s\lambda_2\eta} + 2E_3 p_6 e^{s\lambda_3\eta} - E_4 p_1 e^{-s\lambda_1\eta} - 2E_5 p_4 e^{-s\lambda_2\eta} - 2E_6 p_6 e^{-s\lambda_3\eta}\} \\
E_{11\varphi} &= -\frac{1}{2QD}\{E_1 p_2 e^{s\lambda_1\eta} + 2E_2 p_5 e^{s\lambda_2\eta} + 2E_3 p_7 e^{s\lambda_3\eta} - E_4 p_2 e^{-s\lambda_1\eta} - 2E_5 p_5 e^{-s\lambda_2\eta} - 2E_6 p_7 e^{-s\lambda_3\eta}\} \\
E_{12x} &= \frac{1}{2Q'D}\{2E_7 q_1' e^{s\lambda_1\eta} + E_8 q_2' e^{s\lambda_2\eta} + 2E_9 q_3' e^{s\lambda_3\eta} + 2E_{10} q_1' e^{-s\lambda_1\eta} + E_{11} q_2' e^{-s\lambda_2\eta} + 2E_{12} q_3' e^{-s\lambda_3\eta}\} \\
E_{12y} &= -\frac{1}{2QD}\{2E_7 p_1 e^{s\lambda_1\eta} + E_8 p_4 e^{s\lambda_2\eta} + 2E_9 p_6 e^{s\lambda_3\eta} - 2E_{10} p_1 e^{-s\lambda_1\eta} - E_{11} p_4 e^{-s\lambda_2\eta} - 2E_{12} p_6 e^{-s\lambda_3\eta}\} \\
E_{12\varphi} &= -\frac{1}{2QD}\{2E_7 p_2 e^{s\lambda_1\eta} + E_8 p_5 e^{s\lambda_2\eta} + 2E_9 p_7 e^{s\lambda_3\eta} - 2E_{10} p_2 e^{-s\lambda_1\eta} - E_{11} p_5 e^{-s\lambda_2\eta} - 2E_{12} p_7 e^{-s\lambda_3\eta}\} \\
E_{13x} &= \frac{1}{2Q'D}\{2E_{13} q_1' e^{s\lambda_1\eta} + 2E_{14} q_2' e^{s\lambda_2\eta} + E_{15} q_3' e^{s\lambda_3\eta} + 2E_{16} q_1' e^{-s\lambda_1\eta} + 2E_{17} q_2' e^{-s\lambda_2\eta} + E_{18} q_3' e^{-s\lambda_3\eta}\} \\
E_{13y} &= -\frac{1}{2QD}\left\{2E_{13} p_1 e^{s\lambda_1\eta} + 2E_{14} p_4 e^{s\lambda_2\eta} + E_{15} p_6 e^{s\lambda_3\eta} - 2E_{16} p_1 e^{-s\lambda_1\eta} - 2E_{17} p_4 e^{-s\lambda_2\eta} - E_{18} p_6 e^{-s\lambda_3\eta}\right\} \\
E_{13\varphi} &= -\frac{1}{2QD}\{2E_{13} p_2 e^{s\lambda_1\eta} + 2E_{14} p_5 e^{s\lambda_2\eta} + E_{15} p_7 e^{s\lambda_3\eta} - 2E_{16} p_2 e^{-s\lambda_1\eta} - 2E_{17} p_5 e^{-s\lambda_2\eta} - E_{18} p_7 e^{-s\lambda_3\eta}\} \\
F_{11x} &= \frac{1}{2Q'D}\{F_1 q_1' e^{s\lambda_1\eta} + 2F_2 q_2' e^{s\lambda_2\eta} + 2F_3 q_3' e^{s\lambda_3\eta} + F_4 q_1' e^{-s\lambda_1\eta} + 2F_5 q_2' e^{-s\lambda_2\eta} + 2F_6 q_3' e^{-s\lambda_3\eta}\} \\
F_{11y} &= -\frac{1}{2QD}\{F_1 p_1 e^{s\lambda_1\eta} + 2F_2 p_4 e^{s\lambda_2\eta} + 2F_3 p_6 e^{s\lambda_3\eta} - F_4 p_1 e^{-s\lambda_1\eta} - 2F_5 p_4 e^{-s\lambda_2\eta} - 2F_6 p_6 e^{-s\lambda_3\eta}\} \\
F_{11\varphi} &= -\frac{1}{2QD}\{F_1 p_2 e^{s\lambda_1\eta} + 2F_2 p_5 e^{s\lambda_2\eta} + 2F_3 p_7 e^{s\lambda_3\eta} - F_4 p_2 e^{-s\lambda_1\eta} - 2F_5 p_5 e^{-s\lambda_2\eta} - 2F_6 p_7 e^{-s\lambda_3\eta}\} \\
F_{12x} &= \frac{1}{2Q'D}\{2F_7 q_1' e^{s\lambda_1\eta} + F_8 q_2' e^{s\lambda_2\eta} + 2F_9 q_3' e^{s\lambda_3\eta} + 2F_{10} q_1' e^{-s\lambda_1\eta} + F_{11} q_2' e^{-s\lambda_2\eta} + 2F_{12} q_3' e^{-s\lambda_3\eta}\} \\
F_{12y} &= -\frac{1}{2QD}\{2F_7 p_1 e^{s\lambda_1\eta} + F_8 p_4 e^{s\lambda_2\eta} + 2F_9 p_6 e^{s\lambda_3\eta} - 2F_{10} p_1 e^{-s\lambda_1\eta} - F_{11} p_4 e^{-s\lambda_2\eta} - 2F_{12} p_6 e^{-s\lambda_3\eta}\} \\
F_{12\varphi} &= -\frac{1}{2QD}\{2F_7 p_2 e^{s\lambda_1\eta} + F_8 p_5 e^{s\lambda_2\eta} + 2F_9 p_7 e^{s\lambda_3\eta} - 2F_{10} p_2 e^{-s\lambda_1\eta} - F_{11} p_5 e^{-s\lambda_2\eta} - 2F_{12} p_7 e^{-s\lambda_3\eta}\} \\
F_{13x} &= \frac{1}{2Q'D}\{-2F_{13} q_1' e^{s\lambda_1\eta} + 2F_{14} q_2' e^{s\lambda_2\eta} + F_{15} q_3' e^{s\lambda_3\eta} + 2F_{16} q_1' e^{-s\lambda_1\eta} + 2F_{17} q_2' e^{-s\lambda_2\eta} + F_{18} q_3' e^{-s\lambda_3\eta}\} \\
F_{13y} &= -\frac{1}{2QD}\{-2F_{13} p_1 e^{s\lambda_1\eta} + 2F_{14} p_4 e^{s\lambda_2\eta} + F_{15} p_6 e^{s\lambda_3\eta} - 2F_{16} p_1 e^{-s\lambda_1\eta} - 2F_{17} p_4 e^{-s\lambda_2\eta} - F_{18} p_6 e^{-s\lambda_3\eta}\} \\
F_{13\varphi} &= -\frac{1}{2QD}\{-2F_{13} p_2 e^{s\lambda_1\eta} + 2F_{14} p_5 e^{s\lambda_2\eta} + F_{15} p_7 e^{s\lambda_3\eta} - 2F_{16} p_2 e^{-s\lambda_1\eta} - 2F_{17} p_5 e^{-s\lambda_2\eta} - F_{18} p_7 e^{-s\lambda_3\eta}\}
\end{aligned} \tag{A.2}
$$

where

$$D(s)=q_1[e^{-2|s|(\lambda_1+\lambda_2+\lambda_3)h}+e^{-2|s|(\lambda_2+\lambda_3)h}-e^{-2|s|(\lambda_1+\lambda_3)h}+e^{-2|s|(\lambda_1+\lambda_2)h}-e^{-2|s|\lambda_1h}+e^{-2|s|\lambda_2h}-e^{-2|s|\lambda_3h}$$
$$+8(\frac{q_5}{q_1})(e^{-|s|(\lambda_1+\lambda_2+2\lambda_3)h}-e^{-|s|(\lambda_1+\lambda_2)h})-4(e^{-|s|(\lambda_1+2\lambda_2+\lambda_3)h}-e^{-|s|(\lambda_1+\lambda_3)h})$$
$$+8(\frac{q_7}{q_1})(e^{-|s|(2\lambda_1+\lambda_2+\lambda_3)h}-e^{-|s|(\lambda_2+\lambda_3)h})-1]$$
$$E_1(s)=q_1(e^{-2s(\lambda_1+\lambda_3)h}+e^{-2s\lambda_1h}-e^{-2s(\lambda_1+\lambda_2)h}-e^{-2s(\lambda_1+\lambda_2+\lambda_3)h}-2e^{-s(\lambda_1+\lambda_3)h}+2e^{-s(\lambda_1+2\lambda_2+\lambda_3)h})$$
$$-8q_3e^{-s(2\lambda_1+\lambda_2+\lambda_3)h}+4q_2(e^{-s(\lambda_1+\lambda_2)h}-e^{-s(\lambda_1+\lambda_2+2\lambda_3)h})$$
$$E_2(s)=q_4(e^{-2s\lambda_2h}+e^{-s(\lambda_1+\lambda_2+2\lambda_3)h})-q_5(e^{-2s(\lambda_2+\lambda_3)h}+e^{-s(\lambda_1+\lambda_2)h})+2q_6(e^{-s(\lambda_2+\lambda_3)h}+e^{-s(\lambda_1+2\lambda_2+\lambda_3)h})$$
$$E_3(s)=-q_7(e^{-s(\lambda_1+\lambda_3)h}+e^{-2s(\lambda_2+\lambda_3)h})+q_8(e^{-s(\lambda_1+2\lambda_2+\lambda_3)h}+e^{-2s\lambda_3h})+2q_9(e^{-s(\lambda_2+\lambda_3)h}+e^{-s(\lambda_1+\lambda_2+2\lambda_3)h})$$
$$E_4(s)=-8q_3e^{-s(\lambda_2+\lambda_3)h}q_{10}(1+e^{-2s(\lambda_2+\lambda_3)h})-q_{11}(e^{-2s\lambda_2h}+e^{-2s\lambda_3h})$$
$$E_5(s)=2q_6(e^{-s(\lambda_1+\lambda_3)h}+e^{-s(\lambda_2+\lambda_3)h})+q_{14}(e^{-2s\lambda_3h}+e^{-s(\lambda_1+\lambda_2)h})-q_{15}(1+e^{-|s|(\lambda_1+\lambda_2+2\lambda_3)h})$$
$$E_6(s)=-q_{12}(1+e^{-s(\lambda_1+2\lambda_2+\lambda_3)h})+q_{13}(e^{-2s\lambda_2h}+e^{-s(\lambda_1+\lambda_3)h})+2q_9(e^{-s(\lambda_2+\lambda_3)h}+e^{-s(\lambda_1+\lambda_2)h})$$
$$E_7(s)=q_{16}(e^{-2s\lambda_1h}+e^{-s(\lambda_1+\lambda_2+2\lambda_3)h})-q_{17}(e^{-2s(\lambda_1+\lambda_3)h}+e^{-s(\lambda_1+\lambda_2)h})-2q_{18}(e^{-s(\lambda_1+\lambda_3)h}+e^{-s(2\lambda_1+\lambda_2+\lambda_3)h})$$
$$E_8(s)=-q_1(e^{-2s(\lambda_2+\lambda_3)h}+e^{-2s\lambda_2h}+e^{-2s(\lambda_1+\lambda_2)h}+e^{-2s(\lambda_1+\lambda_2+\lambda_3)h}-4e^{-s(\lambda_1+2\lambda_2+\lambda_3)h})$$
$$+4q_2(e^{-s(\lambda_1+\lambda_2)h}-e^{-s(\lambda_1+\lambda_2+2\lambda_3)h})+4q_3(e^{-s(\lambda_2+\lambda_3)h}-e^{-s(2\lambda_1+\lambda_2+\lambda_3)h})$$
$$E_9(s)=2q_{19}(e^{-s(\lambda_1+\lambda_2+2\lambda_3)h}+e^{-s(\lambda_1+\lambda_3)h})+q_{20}(e^{-2s\lambda_3h}+e^{-s(2\lambda_1+\lambda_2+\lambda_3)h})-q_{21}(e^{-2s(\lambda_1+\lambda_3)h}+e^{-s(\lambda_2+\lambda_3)h})$$
$$E_{10}(s)=-2q_{18}(e^{-s(\lambda_2+\lambda_3)h}+e^{-s(\lambda_1+\lambda_3)h})-q_{22}(1+e^{-s(\lambda_1+\lambda_2+2\lambda_3)h})+q_{23}(e^{-2s\lambda_3h}+e^{-s(\lambda_1+\lambda_2)h})$$
$$E_{11}(s)=-q_1(1+e^{-2s\lambda_2)h}+4e^{-s(\lambda_1+\lambda_3)h}-e^{-2s\lambda_1h}-e^{-2s\lambda_3h})$$
$$E_{12}(s)=2q_{19}e^{-s(\lambda_1+\lambda_3)h}+2q_{20}e^{-s(\lambda_1+\lambda_2)h}-q_{24}(1+e^{-s(2\lambda_1+\lambda_2+\lambda_3)h})+q_{25}(e^{-2s\lambda_1h}+e^{-s(\lambda_2+\lambda_3)h})$$
$$-q_{26}e^{-2s(\lambda_2+\lambda_3)h}$$
$$E_{13}(s)=-q_{27}(e^{-s(\lambda_1+\lambda_3)h}+e^{-2s(\lambda_1+\lambda_2)h})+q_{28}(e^{-s(\lambda_1+2\lambda_2+\lambda_3)h}+e^{-2s\lambda_1h})+2q_{29}(e^{-s(\lambda_1+\lambda_2)h}+e^{-s(2\lambda_1+\lambda_2+\lambda_3)h})$$
$$E_{14}(s)=q_{30}(e^{-s(2\lambda_1+\lambda_2+\lambda_3)h}+e^{-2s\lambda_2h}-e^{-s(\lambda_2+\lambda_3)h}-e^{-2s(\lambda_1+\lambda_2)h})+2q_{31}(e^{-s(\lambda_1+\lambda_2)h}+e^{-s(\lambda_1+2\lambda_2+\lambda_3)h})$$
$$E_{15}(s)=-q_1(e^{-2s(\lambda_2+\lambda_3)h}-e^{-2s\lambda_3h}-e^{-2s(\lambda_1+\lambda_3)h}+e^{-2s(\lambda_1+\lambda_2+\lambda_3)h}-2e^{-s(\lambda_1+2\lambda_2+\lambda_3)h}+2e^{-s(\lambda_1+\lambda_3)h})$$
$$-8q_2e^{-s(\lambda_1+\lambda_2+2\lambda_3)h}-4q_3(e^{-s(2\lambda_1+\lambda_2+\lambda_3)h}-e^{-s(\lambda_2+\lambda_3)h})$$
$$E_{16}(s)=2q_{29}(e^{-s(\lambda_2+\lambda_3)h}+e^{-s(\lambda_1+\lambda_2)h})+q_{32}(1+e^{-s(\lambda_1+2\lambda_2+\lambda_3)h})+q_{33}(e^{-2s\lambda_2h}+e^{-s(\lambda_1+\lambda_3)h})$$
$$E_{17}(s)=-q_{34}(e^{-s(\lambda_2+\lambda_3)h}+e^{-2s\lambda_1h})+q_{35}(e^{-s(2\lambda_1+\lambda_2+\lambda_3)h}+1)-2q_{36}(e^{-s(\lambda_1+\lambda_3)h}+e^{-s(\lambda_1+\lambda_2)h})$$
$$E_{18}(s)=-8q_2e^{-s(\lambda_1+\lambda_2)h}-q_{37}(1+e^{-2s(\lambda_1+\lambda_2)h})+q_{38}(e^{-2s\lambda_1h}+e^{-2s\lambda_2h})$$
$$F_1(s)=8q_3e^{-s(2\lambda_1+\lambda_2+\lambda_3)h}-q_{10}(e^{-2s\lambda_1h}+e^{-2s(\lambda_1+\lambda_2+\lambda_3)h})+q_{11}(e^{-2s(\lambda_1+\lambda_3)h}+e^{-2s(\lambda_1+\lambda_2)h})$$
$$F_2(s)=-2q_6(e^{-s(2\lambda_1+\lambda_2+\lambda_3)h}+e^{-s(\lambda_1+2\lambda_2+\lambda_3)h})-q_{14}(e^{-2s(\lambda_1+\lambda_2)h}+e^{-s(\lambda_1+\lambda_2+2\lambda_3)h})$$
$$+q_{15}(e^{-2s(\lambda_1+\lambda_2+\lambda_3)h}+e^{-s(\lambda_1+\lambda_2)h})$$
$$F_3(s)=-2q_9(e^{-s(\lambda_1+\lambda_2+2\lambda_3)h}+e^{-s(2\lambda_1+\lambda_2+\lambda_3)h})+q_{12}(e^{-s(\lambda_1+\lambda_3)h}+e^{-2s(\lambda_1+\lambda_2+\lambda_3)h})$$
$$+q_{13}(e^{-2s(\lambda_1+\lambda_3)h}+e^{-s(\lambda_1+2\lambda_2+\lambda_3)h})$$
$$F_4(s)=q_1(1-e^{-2s(\lambda_2+\lambda_3)h}+e^{-2s\lambda_3h}-e^{-2s\lambda_2h}+2e^{-s(\lambda_1+2\lambda_2+\lambda_3)h}-2e^{-s(\lambda_1+\lambda_3)h})$$
$$-4q_2(e^{-s(\lambda_1+\lambda_2+2\lambda_3)h}-e^{-s(\lambda_1+\lambda_2)h})+8q_3e^{-s(\lambda_2+\lambda_3)h}$$
$$F_5(s)=-q_4(e^{-2s(\lambda_1+\lambda_3)h}+e^{-s(\lambda_1+\lambda_2)h})+q_5(e^{-s(\lambda_1+\lambda_2+2\lambda_3)h}+e^{-2s\lambda_1h})-2q_6(e^{-s(2\lambda_1+\lambda_2+\lambda_3)h}+e^{-s(\lambda_1+\lambda_3)h})$$
$$F_6(s)=q_7(e^{-s(\lambda_1+2\lambda_2+\lambda_3)h}+e^{-2s\lambda_1h})-q_8(e^{-2s(\lambda_1+\lambda_2)h}+e^{-s(\lambda_1+\lambda_3)h})-2q_9(e^{-s(\lambda_1+\lambda_2)h}+e^{-s(2\lambda_1+\lambda_2+\lambda_3)h})$$

$$
\begin{aligned}
F_7(s) &= q_{22}(e^{-s(\lambda_1+\lambda_2)h} + e^{-2s(\lambda_1+\lambda_2+\lambda_3)h}) - q_{23}(e^{-s(\lambda_1+\lambda_2+2\lambda_3)h} + e^{-2s(\lambda_1+\lambda_2)h}) \\
&\quad -2q_{33}(e^{-s(\lambda_1+2\lambda_2+\lambda_3)h} + e^{-s(2\lambda_1+\lambda_2+\lambda_3)h}) \\
F_8(s) &= q_1(e^{-2s(\lambda_2+\lambda_3)h} + e^{-2s(\lambda_1+\lambda_2)h} + e^{-2s(\lambda_1+\lambda_2+\lambda_3)h} + e^{-2s\lambda_2 h} - 4e^{-s(\lambda_1+2\lambda_2+\lambda_3)h}) \\
F_9(s) &= 2q_{19}(e^{-s(\lambda_1+\lambda_2+2\lambda_3)h} - e^{-s(\lambda_1+2\lambda_2+\lambda_3)h}) + q_{24}(e^{-s(\lambda_2+\lambda_3)h} + e^{-2s(\lambda_1+\lambda_2+\lambda_3)h}) \\
&\quad -q_{25}(e^{-2s(\lambda_2+\lambda_3)h} + e^{-s(2\lambda_1+\lambda_2+\lambda_3)h}) \\
F_{10}(s) &= -q_{16}(e^{-2s(\lambda_2+\lambda_3)h} + e^{-s(\lambda_1+\lambda_2)h}) + q_{17}(e^{-s(\lambda_1+\lambda_2+2\lambda_3)h} + e^{-2s\lambda_2 h}) + 2q_{18}(e^{-s(\lambda_1+2\lambda_2+\lambda_3)h} + e^{-s(\lambda_2+\lambda_3)h}) \\
F_{11}(s) &= q_1(1 + e^{-2s(\lambda_1+\lambda_3)h} + e^{-2s\lambda_3 h} + e^{-2s\lambda_1 h} - 4e^{-s(\lambda_1+\lambda_3)h}) + 4q_2(e^{-s(\lambda_1+\lambda_2+2\lambda_3)h} + e^{-s(\lambda_1+\lambda_2)h}) \\
&\quad -4q_3(e^{-s(2\lambda_1+\lambda_2+\lambda_3)h} - e^{-s(\lambda_2+\lambda_3)h}) \\
F_{12}(s) &= -q_{21}(e^{-2s(\lambda_1+\lambda_2)h} + e^{-s(\lambda_2+\lambda_3)h}) + q_{22}(e^{-s(2\lambda_1+\lambda_2+\lambda_3)h} + e^{-2s\lambda_2 h}) - 2q_{39}(e^{-s(\lambda_1+2\lambda_2+\lambda_3)h} + e^{-s(\lambda_1+\lambda_2)h}) \\
F_{13}(s) &= 2q_{29}(e^{-s(\lambda_1+\lambda_2+2\lambda_3)h} + e^{-s(2\lambda_1+\lambda_2+\lambda_3)h}) + q_{32}(e^{-s(\lambda_1+\lambda_3)h} + e^{-2s(\lambda_1+\lambda_2+\lambda_3)h}) \\
&\quad +q_{33}(e^{-2s(\lambda_1+\lambda_3)h} + e^{-s(\lambda_1+2\lambda_2+\lambda_3)h}) \\
F_{14}(s) &= -2q_{31}(e^{-s(\lambda_1+\lambda_2+2\lambda_3)h} + e^{-s(\lambda_1+2\lambda_2+\lambda_3)h}) + q_{34}(e^{-2s(\lambda_2+\lambda_3)h} + e^{-s(2\lambda_1+\lambda_2+\lambda_3)h}) \\
&\quad -q_{35}(e^{-2s(\lambda_1+\lambda_2+\lambda_3)h} + e^{-s(\lambda_2+\lambda_3)h}) \\
F_{15}(s) &= 8q_2 e^{-s(\lambda_1+\lambda_2+2\lambda_3)h} + q_{37}(e^{-2s\lambda_3 h} + e^{-2s(\lambda_1+\lambda_2+\lambda_3)h}) - q_{38}(e^{-2s(\lambda_2+\lambda_3)h} + e^{-2s(\lambda_1+\lambda_3)h}) \\
F_{16}(s) &= q_{27}(e^{-s(\lambda_1+2\lambda_2+\lambda_3)h} + e^{-2s\lambda_3 h}) - q_{28}(e^{-2s(\lambda_2+\lambda_3)h} + e^{-s(\lambda_1+\lambda_3)h}) - 2q_{29}(e^{-s(\lambda_1+\lambda_2+2\lambda_3)h} + e^{-s(\lambda_2+\lambda_3)h}) \\
F_{17}(s) &= q_{30}(e^{-s(2\lambda_1+\lambda_2+\lambda_3)h} + e^{-2s\lambda_3 h} - e^{-2s(\lambda_1+\lambda_3)h} - e^{-s(\lambda_2+\lambda_3)h}) - 2q_{31}(e^{-s(\lambda_1+\lambda_2+2\lambda_3)h} + e^{-s(\lambda_1+\lambda_3)h}) \\
F_{18}(s) &= -q_1(e^{-2s(\lambda_1+\lambda_2)h} + 2e^{-s(\lambda_1+\lambda_3)h} - 2e^{-s(\lambda_1+2\lambda_2+\lambda_3)h} + e^{-2s\lambda_2 h} - e^{-2s\lambda_1 h} - 1) + 8q_2 e^{-s(\lambda_1+\lambda_2)h} \\
&\quad +4q_3(e^{-s(\lambda_2+\lambda_3)h} - e^{-s(2\lambda_1+\lambda_2+\lambda_3)h})
\end{aligned} \tag{A.3}
$$

and

$$p_1 = m_{22}m_{35} - m_{25}m_{32}, \quad p_2 = m_{25}m_{31} - m_{21}m_{35}, \quad p_3 = m_{21}m_{32} - m_{22}m_{31},$$

$$p_4 = m_{15}m_{32} - m_{12}m_{35}, \quad p_5 = m_{11}m_{35} - m_{15}m_{31},$$

$$p_6 = m_{12}m_{25} - m_{15}m_{22}, \quad p_7 = m_{15}m_{21} - m_{11}m_{25},$$

$$q_1' = m_{24}m_{37} - m_{27}m_{34}, \quad q_2' = m_{17}m_{34} - m_{14}m_{37}, \quad q_3' = m_{14}m_{27} - m_{17}m_{24},$$

$$Q = m_{11}p_1 + m_{12}p_2 + m_{15}p_3, \quad Q' = q_1' + q_2' + q_3'$$

$$
\begin{aligned}
q_1 &= n_1 + n_2 + n_3 + n_4 + n_5 + n_6 - 2n_7 - 2n_8 - 2n_9 - 2n_{10} - 2n_{11} - 2n_{12} - 2n_{13} - 2n_{14} - 2n_{15} \\
&\quad +2n_{16} + 2n_{17} + 2n_{18} + 2n_{19} + 2n_{20} + 2n_{21},
\end{aligned}
$$

$$q_2 = n_7 + n_9 - n_{17} - n_{21}, \quad q_3 = n_{13} + n_{15} - n_{18} - n_{19},$$

$$q_4 = n_{22} + n_{23} + n_{24} + n_{25} - n_{30} - n_{32} - n_{33} - n_{34} + n_{38} + n_{39} - 2n_{40},$$

$$q_5 = n_{22} + n_{23} + n_{24} + n_{25} + n_{30} + n_{32} - n_{33} - n_{34} - n_{38} - n_{39} - 2n_{40}, \quad q_6 = n_{30} + n_{32} - n_{38} - n_{39},$$

$$q_7 = n_{26} + n_{27} + n_{28} + n_{29} + n_{31} - n_{35} - n_{36} + n_{37} - n_{41} - n_{42} - 2n_{43},$$

$$q_8 = n_{26} + n_{27} + n_{28} + n_{29} - n_{31} - n_{35} - n_{36} - n_{37} + n_{41} + n_{42} - 2n_{43}, \quad q_9 = n_{31} + n_{37} - n_{41} - n_{42},$$

$$q_{10} = n_1 - n_2 - n_3 - n_4 + n_5 - n_6 + 2n_8 + 2n_{11} + 2n_{13} - 2n_{14} + 2n_{15} - 2n_{18} - 2n_{19},$$

$$q_{11} = n_1 - n_2 - n_3 - n_4 + n_5 - n_6 + 2n_8 + 2n_{11} - 2n_{13} - 2n_{14} - 2n_{15} + 2n_{18} + 2n_{19},$$

$$q_{12}=n_{26}-n_{27}-n_{28}+n_{29}+n_{31}-n_{35}-n_{36}+n_{37}-n_{41}-n_{42}+2n_{43},$$
$$q_{13}=n_{26}-n_{27}-n_{28}+n_{29}-n_{31}-n_{35}-n_{36}-n_{37}+n_{41}+n_{42}+2n_{43},$$
$$q_{14}=n_{22}-n_{23}-n_{24}+n_{25}-n_{30}-n_{32}-n_{33}-n_{34}+n_{38}+n_{39}+2n_{40},$$
$$q_{15}=n_{22}-n_{23}-n_{24}+n_{25}+n_{30}+n_{32}-n_{33}-n_{34}-n_{38}-n_{39}+2n_{40},$$
$$q_{16}=n_{44}+n_{45}+n_{46}+n_{47}-n_{52}-n_{53}-n_{54}-n_{55}+n_{61}+n_{62}-2n_{63},$$
$$q_{17}=n_{44}+n_{45}+n_{46}+n_{47}+n_{52}-n_{53}+n_{54}-n_{55}-n_{61}-n_{62}-2n_{63},$$
$$q_{18}=-n_{52}-n_{54}+n_{61}+n_{62},\quad q_{19}=n_{58}+n_{59}-n_{64}-n_{66},$$
$$q_{20}=-n_{59}+n_{48}+n_{49}+n_{50}+n_{51}-n_{56}-n_{57}-n_{58}+n_{64}-2n_{65}+n_{66},$$
$$q_{21}=n_{59}+n_{48}+n_{49}+n_{50}+n_{51}-n_{56}-n_{57}+n_{58}-n_{64}-2n_{65}-n_{66},$$
$$q_{22}=n_{44}-n_{45}-n_{46}+n_{47}+n_{52}-n_{53}+n_{54}-n_{55}-n_{61}-n_{62}+2n_{63},$$
$$q_{23}=n_{44}-n_{45}-n_{46}+n_{47}-n_{52}-n_{53}-n_{54}-n_{55}+n_{61}+n_{62}+2n_{63},$$
$$q_{24}=n_{48}-n_{49}-n_{50}+n_{51}-n_{56}-n_{57}+n_{58}+n_{59}-n_{64}+2n_{65}-n_{66},$$
$$q_{25}=n_{48}-n_{49}-n_{50}+n_{51}-n_{56}-n_{57}-n_{58}-n_{59}+n_{64}+2n_{65}+n_{66},\quad q_{26}=n_{50}+n_{58},$$
$$q_{27}=n_{70}+n_{71}+n_{72}+n_{73}+n_{78}-n_{79}-n_{80}+n_{81}-n_{85}-2n_{86}-n_{87},$$
$$q_{28}=n_{70}+n_{71}+n_{72}+n_{73}-n_{78}-n_{79}-n_{80}-n_{81}+n_{85}-2n_{86}+n_{87},$$
$$q_{29}=n_{78}+n_{81}-n_{85}-n_{87},\quad q_{30}=n_{60}+n_{67}+n_{68}+n_{69}+n_{74}-n_{75}-n_{76}+n_{77}-n_{82}-2n_{83}-n_{84},$$
$$q_{31}=n_{74}+n_{77}-n_{82}-n_{84},\quad q_{32}=-n_{70}+n_{71}+n_{72}-n_{73}-n_{88}+n_{79}+n_{80}-n_{81}+n_{85}-2n_{86}+n_{87},$$
$$q_{33}=n_{70}-n_{71}-n_{72}+n_{73}-n_{78}-n_{79}-n_{80}-n_{81}+n_{85}+2n_{86}+n_{87},$$
$$q_{34}=-n_{60}+n_{67}+n_{68}-n_{69}+n_{74}+n_{75}+n_{76}+n_{77}-n_{82}-2n_{83}-n_{84},$$
$$q_{35}=-n_{60}+n_{67}+n_{68}-n_{69}-n_{74}+n_{75}+n_{76}-n_{77}+n_{82}-2n_{83}+n_{84},\quad q_{36}=-n_{74}-n_{77}+n_{82}+n_{84},$$
$$q_{37}=n_1+n_2-n_3-n_4+n_5+n_6-2n_7+2n_8-2n_9-2n_{11}-2n_{14}+2n_{17}+2n_{21},$$
$$q_{38}=n_1+n_2-n_3-n_4+n_5+n_6+2n_7+2n_8+2n_9-2n_{11}-2n_{14}-2n_{17}-2n_{21},$$
$$q_{39}=-n_{49}-n_{50}-n_{51}+n_{57}+n_{58}-n_{64}+2n_{65} \tag{A.4}$$

In which

$$n_1=m_{15}^2m_{24}^2m_{37}^2,\quad n_2=m_{17}^2m_{25}^2m_{34}^2,\quad n_3=m_{17}^2m_{24}^2m_{35}^2,\quad n_4=m_{14}^2m_{27}^2m_{35}^2,\quad n_5=m_{15}^2m_{27}^2m_{34}^2$$
$$n_6=m_{14}^2m_{25}^2m_{37}^2,\quad n_7=m_{14}m_{15}m_{24}m_{25}m_{37}^2,\quad n_8=m_{14}m_{17}m_{24}m_{27}m_{35}^2,\quad n_9=m_{15}m_{17}m_{25}m_{27}m_{34}^2$$
$$n_{10}=m_{14}m_{15}m_{27}^2m_{34}m_{35},\quad n_{11}=m_{14}m_{17}m_{25}^2m_{34}m_{37},\quad n_{12}=m_{15}m_{17}m_{24}^2m_{35}m_{37},$$
$$n_{13}=m_{17}^2m_{24}m_{25}m_{34}m_{35}$$
$$n_{14}=m_{15}^2m_{24}m_{27}m_{34}m_{37},\quad n_{15}=m_{14}^2m_{25}m_{27}m_{35}m_{37},\quad n_{16}=m_{14}m_{15}m_{24}m_{27}m_{35}m_{37},$$
$$n_{17}=m_{14}m_{15}m_{25}m_{27}m_{34}m_{37}$$
$$n_{18}=m_{14}m_{17}m_{24}m_{25}m_{35}m_{37},\quad n_{19}=m_{14}m_{17}m_{25}m_{27}m_{34}m_{35},\quad n_{20}=m_{15}m_{17}m_{24}m_{27}m_{34}m_{35},$$
$$n_{21}=m_{15}m_{17}m_{24}m_{25}m_{34}m_{37},\quad n_{22}=m_{14}m_{24}m_{25}^2m_{37}^2,\quad n_{23}=m_{15}m_{25}m_{27}^2m_{34}^2$$
$$n_{24}=m_{15}m_{24}^2m_{25}m_{37}^2,\quad n_{25}=m_{17}m_{25}^2m_{27}m_{34}^2,\quad n_{26}=m_{14}m_{27}^2m_{34}m_{35}^2,\quad n_{27}=m_{15}m_{24}^2m_{35}m_{37}^2$$
$$n_{28}=m_{15}m_{27}^2m_{34}^2m_{35},\quad n_{29}=m_{17}m_{24}^2m_{35}^2m_{37},\quad n_{30}=m_{14}m_{25}m_{27}^2m_{34}m_{35},$$
$$n_{31}=m_{14}m_{24}m_{25}m_{35}m_{37}^2,\quad n_{32}=m_{17}m_{24}^2m_{25}m_{35}m_{37},\quad n_{33}=m_{14}m_{25}^2m_{27}m_{34}m_{37},$$
$$n_{34}=m_{17}m_{24}m_{25}^2m_{34}m_{37}$$
$$n_{35}=m_{14}m_{24}m_{27}m_{35}^2m_{37},\quad n_{36}=m_{17}m_{24}m_{27}m_{34}m_{35}^2,\quad n_{37}=m_{17}m_{25}m_{27}m_{34}^2m_{35},$$
$$n_{38}=m_{14}m_{24}m_{25}m_{27}m_{35}m_{37},\quad n_{39}=m_{17}m_{24}m_{25}m_{27}m_{34}m_{35},\quad n_{40}=m_{15}m_{24}m_{25}m_{27}m_{34}m_{37},$$
$$n_{41}=m_{14}m_{25}m_{27}m_{34}m_{35}m_{37},\quad n_{42}=m_{17}m_{24}m_{25}m_{34}m_{35}m_{37},\quad n_{43}=m_{15}m_{24}m_{27}m_{34}m_{35}m_{37},$$
$$n_{44}=m_{14}m_{15}^2m_{24}m_{37}^2,\quad n_{45}=m_{15}m_{17}^2m_{25}m_{34}^2,\quad n_{46}=m_{14}^2m_{15}m_{25}m_{37}^2,\quad n_{47}=m_{15}^2m_{17}m_{27}m_{34}^2,$$

$$\begin{gathered}
n_{48}=m_{17}^2m_{24}m_{34}m_{35}^2,\quad n_{49}=m_{14}^2m_{25}m_{35}m_{37}^2,\quad n_{50}=m_{17}^2m_{25}m_{34}^2m_{35},\quad n_{51}=m_{14}^2m_{27}m_{35}^2m_{37},\\
n_{52}=m_{15}m_{17}^2m_{24}m_{34}m_{35},\quad n_{53}=m_{14}m_{15}^2m_{27}m_{34}m_{37},\quad n_{54}=m_{14}^2m_{15}m_{27}m_{35}m_{37},\\
n_{55}=m_{15}^2m_{17}m_{24}m_{34}m_{37}\\
n_{56}=m_{14}m_{17}m_{24}m_{35}^2m_{37},\quad n_{57}=m_{14}m_{17}m_{27}m_{34}m_{35}^2,\quad n_{58}=m_{15}m_{17}m_{27}m_{34}^2m_{35},\\
n_{59}=m_{14}m_{15}m_{24}m_{35}m_{37}^2,\quad n_{60}=m_{17}^2m_{24}m_{25}^2m_{34},\quad n_{61}=m_{14}m_{15}m_{17}m_{24}m_{35}m_{37}\\
n_{62}=m_{14}m_{15}m_{17}m_{27}m_{34}m_{35},\quad n_{63}=m_{14}m_{15}m_{17}m_{25}m_{34}m_{37},\quad n_{64}=m_{14}m_{15}m_{27}m_{34}m_{35}m_{37},\\
n_{65}=m_{14}m_{17}m_{25}m_{34}m_{35}m_{37},\quad n_{66}=m_{15}m_{17}m_{24}m_{34}m_{35}m_{37},\quad n_{67}=m_{14}^2m_{25}m_{27}^2m_{35},\\
n_{68}=m_{17}^2m_{24}^2m_{25}m_{35}\\
n_{69}=m_{14}^2m_{25}^2m_{27}m_{37},\quad n_{70}=m_{14}m_{15}^2m_{27}^2m_{34},\quad n_{71}=m_{15}m_{17}^2m_{24}^2m_{35},\quad n_{72}=m_{14}^2m_{15}m_{27}^2m_{35},\\
n_{73}=m_{15}^2m_{17}m_{24}^2m_{37},\quad n_{74}=m_{14}m_{15}m_{25}m_{27}^2m_{34},\quad n_{75}=m_{14}m_{17}m_{24}m_{25}^2m_{37},\quad n_{76}=m_{14}m_{17}m_{25}^2m_{27}m_{34},\\
n_{77}=m_{15}m_{17}m_{24}^2m_{25}m_{37},\quad n_{78}=m_{15}m_{17}^2m_{24}m_{25}m_{34},\quad n_{79}=m_{14}m_{15}^2m_{24}m_{27}m_{37},\\
n_{80}=m_{15}^2m_{17}m_{24}m_{27}m_{37},\\
n_{81}=m_{14}^2m_{15}m_{25}m_{27}m_{37},n_{82}=m_{14}m_{15}m_{24}m_{25}m_{27}m_{37},\quad n_{83}=m_{14}m_{17}m_{24}m_{25}m_{27}m_{35},\\
n_{84}=m_{15}m_{17}m_{24}m_{25}m_{27}m_{34},\\
n_{85}=m_{14}m_{15}m_{17}m_{24}m_{25}m_{37},\quad n_{86}=m_{14}m_{15}m_{17}m_{24}m_{27}m_{35},\quad n_{87}=m_{14}m_{15}m_{17}m_{25}m_{27}m_{34},
\end{gathered}\tag{A.5}$$

References

1. Dineva, P., Muller, D.G.R., Rangelov, T.: Dynamic fracture of piezoelectric materials, solution of time-harmonic problems via BIEM. Springer International Publishing, Switzerland (2014)
2. Tichy, J., Erhart, J., Kittinger, E., Privratska, J.: Fundamentals of piezoelectric sensorics. Springer International Publishing, Verlag Berlin Heidelberg (2010)
3. Hassan, A.M., Alomari, M.A., Alajmi, A., Sadeq, A.M., Alqurashi, F., Flayyih, M.A., Kaza, O.: Numerical analysis of coupled fluid-structure interaction in magnetohydrodynamic flow and phase change process of nano-encapsulated phase change material systems with deformable heated surface. Case Stud. Therm. Eng. **70**, 106131 (2025)
4. Sosa, H.A., Pak, Y.E.: Three-dimensional eigenfunction analysis of a crack in a piezoelectric material. Int. J. Solids Struct. **26**, 1–15 (1990)
5. Zhang, T.Y., Hack, J.E.: Mode-III crack in piezoelectric materials. J. Appl. Phys. **71**, 58–65 (1992)
6. Han, J.J., Chen, Y.H.: Multiple parallel cracks interaction problem in piezoelectric ceramics. Int. J. Solids Struct. **36**, 3375–3390 (1999)
7. Han, X.L., Wang, T.: Interacting multiple cracks in piezoelectric materials. Int. J. Solids Struct. **36**, 4183–4202 (1999)
8. Chao, L.P., Huang, J.H.: Fracture criteria for piezoelectric materials containing multiple cracks. J. Appl. Phys. **85**, 6695–6703 (1999)
9. Gao, C.F.: Further study on the generalized 2D problem of an elliptical hole or a crack in piezoelectric media. Mech. Res. Commun. **27**, 429–434 (2000)
10. Hao, T.H.: Multiple collinear cracks in a piezoelectric material. Int. J. Solids Struct. **38**, 9201–9208 (2001)
11. Yang, F.: Fracture mechanics for mode I crack in piezoelectric materials. Int. J. Solid Struct. **38**, 3813–3830 (2001)
12. Han, J.C., Wang, B.L.: Electromechanical model of periodic cracks in piezoelectric materials. Mech. Mater. **37**, 1180–1197 (2005)
13. Zhou, Z.G., Zhang, P.W., Wu, L.Z.: Two parallel limited-permeable mode-I cracks or four parallel limited-permeable mode-I cracks in the piezoelectric materials. Int. J. Solids Struct. **44**, 4184–4205 (2007)
14. Li, Y.D., Lee, K., Y.: Two collinear unequal cracks in a poled piezoelectric plane: Mode I case solved by a new approach of real fundamental solutions. Int. J. Fract. 165, 47–60 (2010)
15. Monfared, M.M., Ayatollahi, M.: Interactions of multiple cracks in a transversely isotropic piezoelectric plane under mixed mode condition. Eng. Fract. Mech. **180**, 87–104 (2017)
16. Bagheri, R.: Several cracks in a functionally graded piezoelectric plane: in-plane steady harmonic loading case solved by dislocation method. Eng. Fract. Mech. **289**, 109319 (2023)
17. Nourazar, M., Yang, W., Chen, Z.: Fracture analysis of a curved crack in a piezoelectric plane under general thermal loading. Eng. Fract. Mech. **284**, 109208 (2023)
18. Bagheri, R., Ayatollahi, M., Mirzaei, A.M., Monfared, M.M.: Multiple defects in a piezoelectric half-plane under electro-elastic in-plane loadings. Theor. Appl. Fract. Mech. **103**, 102316 (2019)
19. Wang, B.L., Noda, N.: Mixed mode crack initiation in piezoelectric ceramic strip. Theor. Appl. Fract. Mech. **34**, 35–47 (2000)

20. Wang, B.L., Mai, Y.W.: A piezoelectric material strip with a crack perpendicular to its boundary surfaces. Int. J. Solids Struct. **39**, 4501–4524 (2002)
21. Ueda, S.: Thermal intensity factors for a parallel crack in a functionally graded piezoelectric strip. J. Therm. Stress. **30**, 321–342 (2007)
22. Li, X.F.: Closed-form solution for a piezoelectric strip with two collinear cracks normal to the strip boundaries. Eur. J. Mech. **21**, 981–989 (2002)
23. Li, Y.D., Yong, L.K., Feng, F.X., Pan, J.W.: Mode I fracture analysis of a piezoelectric strip based on real fundamental solutions. Eur. J Mech. A/Solids **30**, 158–166 (2011)
24. Yang, W., Nourazar, M., Chen, Z., Hub, K., Zang, X.: Dynamic response of a cracked thermopiezoelectric strip under thermoelectric loading using fractional heat conduction. Appl. Math. Model. **103**, 580–603 (2022)
25. Boroujerdi, R., Monfared, M.M.: Multiple unequal cracks between a functionally graded piezoelectric layer and a piezoelectric substrate by distributed strain nuclei. Comput. Math. Appl. **170**, 116–141 (2024)
26. Weertman, J., Weertman, J.R.: Elementary dislocation theory. Oxford University Press, New York (1992)
27. Faal, R.T., Fariborz, S.J., Daghyani, H.R.: Antiplane deformation of orthotropic strips with multiple defects. J. Mech. Mater. Struct. **1**, 1097–1114 (2006)
28. Ueda, S.: The crack problem in piezoelectric strip under thermoelectric loading. J. Therm. Stresses **29**, 295–316 (2006)
29. Gao, X.Y.: In an ocean or a river: bilinear auto-Backlund transformations and similarity reductions on an extended time dependent (3+1) dimensional shallow water wave equation. China Ocean Eng. **39**, 160–165 (2025)
30. Gao, X.Y.: Hetero-Backland transformations, bilinear and multi-solutions for a (2+1) dimensional generalized modified dispersive water-wave system for the shallow water. Chin. J. of phys. **92**, 1233–1239 (2024)
31. Gao, X.Y.: Open-ocean shallow-water dynamics via a (2+1)-dimensional generalized variable-coefficient Hirota-Satsuma-Ito system: oceanic auto-backlund transformation and oceanic solitons. China Ocean Eng. (2025). https://doi.org/10.1007/s13344-025-0057-y